State University of Londrina (UEL)

Center of Exact Sciences

Department of Physics

Andres David Pardo Perdomo

Optimization of LDS blends of Kb:C7 for applications in the P3HT:PC61BM organic photovoltaic device

Londrina

2019

State University of Londrina (UEL)

Center of Exact Sciences
Department of Physics

Andres David Pardo Perdomo

Optimization of LDS blends of Kb:C7 for applications in the P3HT:PC61BM organic photovoltaic device

Master dissertation oriented by Prof. Dr. Edson Laureto entitled "Optimization of LDS blends of Kb:C7 for applications in the P3HT:PC61BM organic photovoltaic device" and presented to the State University of Londrina (UEL), in partial fulfillment of the requirements for the degree of Master in Physics.

Supervisor: Prof. Dr. Edson Laureto

Londrina
2019

Copyrights

Andres David Pardo Perdomo

Optimization of LDS blends of Kb:C7 for applications in the P3HT:PC61BM organic photovoltaic device

Master dissertation presented to the graduate program: Master in Physics at the State University of Londrina, in partial fulfillment of the requirements for the degree of Master in Physics.

Referees

_____

Prof. Dr. Edson Laureto
State University of Londrina
Advisor

_____

Prof. Dr. Jose Leonil Duarte
State University of Londrina

_____

Prof. Dr. Marco Aurelio Toledo Da Silva
Federal Technological University of Parana

Londrina, September 30, 2019

To those young talented guys who have no opportunities to bright in this unfair world. I dedicate to you the work I carried out by taking advantage of my unique opportunity.

Acknowledgements

To all the members of the Optics and Optoelectronics group. Specially, I am very grateful with Dr. Flavio Franchello for all his positive comments throughout the development of the project. I am also deeply grateful with Professor Jose Leonil Duarte for its helpful support with the time resolved photoluminescence measurements.

To the graduate school at UEL, coordinator of the physics program and administrative staff that help me through all this time.

To Professor Ricardo Vignoto for his concomitant guidance with this work. Apart from the scientific and academic help, he's been an excellent person, a very special friend.

To CAPES and the Brazilian government for funding this research project and for the fellowship given to my for the pursue of my master studies.

To Professor Edson Laureto for being an excellent advisor. For all his scientific and academic support, for trusting in me and for giving me the chance of doing this master project in his lab. More than a scientist, he is a philosopher, a writer and an incomparable human being, a very good example for me.

To all the Brazilian people, in special to those friends and colleagues that I have met during all this time. Thanks for teaching me that beautiful language known as Portuguese. Thanks for the cultural exchange that you let me experience and thanks for hosting me as one of your members.

To all the Colombian friends that have accompanied me through this unique experience. Special thanks to Luis Pinheres and his wife Katia for the unconditional support at the beginning of my master studies. For all the valuable help you provided to me during my first days in Brazil.

To my dear friend and colleague, Johan Diaz, for all the personal and academic support. There is a word that there exist a friend closer than a brother, and without doubts this applies to him. Thanks for trusting in my abilities and furthermore, for the encouragement that I received when it was necessary. Thanks to his dear mother and sister for the reciprocal love and tender.

To my mentor, great master and Professor Ever Ortiz for all his valuable support in the fulfillment of my goals. Without him and his dear wife, this dissertation would be just a dream. Both of them have contributed tremendously throughout my academic life, and they have taught me to never stop dreaming, because from dreams to reality, there is a very small step.

To my cousin Alex Montoya and his family, for being a source of motivation during the critical times. Thanks for being my counselor and my guide when I faced the dark side of this adventure called life.

To my grandfather for his emotive words and for all the emotional support.

To my father, for giving me the life. Although I have shared few time with him, I decided to not living in the past. I owe my whole life to him, and he has turned into my main source of motivation. Thanks for loving me, without regardless of the situation we had faced in the past.

To my mother and aunt, for giving me the life and raising me up, respectively. I personally do not believe in life after death, but it is worth to express gratitude to the women that protected me during the most important years of my life. I am also grateful because they always motivated my scientific and spiritual way, and I am the kind of man I am today thanks to these two women.

To the cosmic artisan, for making those beautiful laws that rule the behaviour of the physical universe.

"If you want to make science, produce knowledge.

If you want to feel good, give others with love.

If you want to make history, produce knowledge, give others with love and be humble."

(Andres Pardo)

Andres David Pardo Perdomo. **Optimization of LDS blends of Kb:C7 for applications in the P3HT:PC61BM organic photovoltaic device**. 2019. 68 p. Master dissertation in Physics - State University of Londrina, Londrina.

Abstract

In this work it is explored the use of two mixed organic dyes, Kremer Blue (Kb) and Coumarin 7 (C7), to design optical filters for applications in the $P3HT : PC_{61}BM$ Organic Photovoltaic device. The use of the filter was intended to increase the External Quantum Efficiency of the device by means of the Luminescent Down-Shifting (LDS) effect, at the same time that is expected to be used for preventing fast UV degradation of the solar cell. It was found that the sample $Kb_{92.5}C7_{7.5}$ dissolved in a PMMA solution (3 mg/mL) has a PLQY of 93.6%, the highest value obtained in the optimization process. Figures of merit of this material, accompanied by simulations of the EQE using the Rothemund model reveal that this sample would contribute to an increment of 19.8% in the photo-generated current of the device. The I-V characteristic curve was measured for eight devices and the average change in current density obtained was 18.6%. Time-resolved PL results show a decrease in the lifetime of samples with different concentrations of C7, compared to the lifetime of single Kb samples. This result suggest that exist an energy transfer process, presumably mediated by a Föster mechanism. The photo-generated current was measured upon solar exposure, with and without the LDS filter, for non encapsulated devices. It was found that during the first 3 hours of solar exposure, the samples with the LDS filter present higher photo-generated current values when compared to devices without the filter. However, upon longer exposure, a rapid drop in the generated current for both devices (with and without filter) was observed. Although increments in the photo-generated current were achieved by means of the LDS filter, further improvements are needed in order to enhance the lifetime of the device.

Key-words: 1. Luminescent Down-Shifting (LDS) effect. 2. Organic photovoltaics. 3. External Quantum Efficiency (EQE). 4. Photoluminescence Qunatum Yield (PLQY). 5.Photo-generated current.

Contents

List of Figures

List of Tables

1 Introduction

1.1 Motivations

It is widely known that most of the amount of energy used by the human being is obtained from non-renewable resources [1]. In fact, roughly 93% of the energy consumed worldwide comes from oil, coal, natural gas and hydro-electrical resources [2]. Unfortunately, extracting those natural resources for satisfying the energy demands of the population has caused a non-repairable damage to the environment, as the effects occasioned by the different processes are not reversible. For example, the global warning, greenhouse effect and the melting of the poles are unavoidable effects that have reached levels beyond the limits of sustainable development. According to the international panel for climate change of the United Nations, if the global temperature continues to increase at the same rates it is increasing nowadays, by 2030 the poles will be completely melted [3]. This information gives us an urgent warning: the life on earth is in danger.
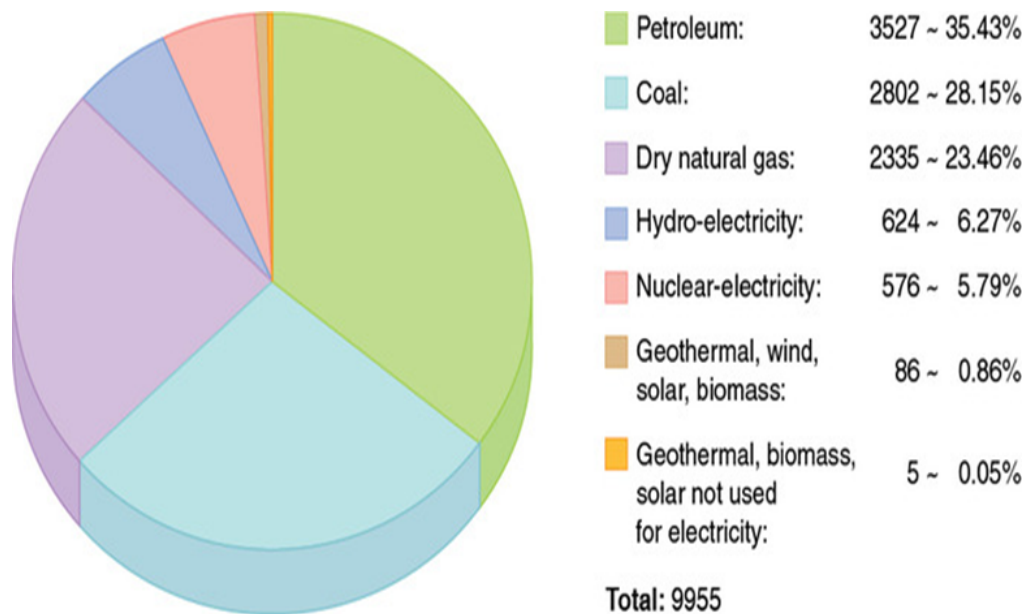
Figure 1 – Distribution of the main sources of energy used by the human being. The percentage of non-renewable resources used for obtaining energy is about 93% [2].

The urgent need of an environment-friendly source of energy has motivated a growing interest within the scientific community to look for alternative and inexpensive ways of obtaining energy. The research in the field of energy transformation and harvesting has

been continuously growing during the last years, and some of the main topics that are been investigated nowadays include: fuel cells, thermo-electrics, super-capacitors, super-conductors, photovoltaics devices and others [4-8].

Nowadays, the commercially dominant photovoltaic technology is that based in Silicon, which has a relatively expensive price and also the fabrication process is very complex. Several emerging technologies are very attractive because of the easy fabrication process and the low cost of production. A few examples are the dyes sensitized solar cells (DSSC) with Grätzel cells, organic-inorganic hybrid perovskites based solar cells and organic solar cells. The main problems of using such technologies are related to the rapid degradation and the low efficiency, which hamper the practical applications of these devices [9]. A great number of alternatives have been explored in order to solve these challenges and make solar cells a costly effective device for producing clean energy. Lately, special attention has been given to perovskites and organic compounds. The low cost of these materials and the low cost techniques required for the synthesis of cells based in these active layers make them very promising candidates for applications in solar cells.

Lately, special attention has been given to Organic Photovoltaic devices (OPV). This type of solar cells offer an additional advantage with respect to the others type of cells: OPV are plastic structures that can be easily manipulated. This property is very useful, as mechanical constraints make difficult the installations of several panels for domestic and industrial applications [10]. The most studied device within OPV materials during the last 10 years is the cell based on poly(3-hexylthiophene-2,5-diyl) (P3HT):phenyl-C61-Butyric-Acid-Methyl Ester (PCBM) ($P3HT : PC_{61}BM$), a bulk heterojunction polymer in which good charge carrier collection is obtained by the interpenetrating network of donor and acceptor materials [11-14].

The main focus in the organic solar cell research lies on increasing the power conversion efficiency [15]. Since it has not yet been possible to replace the C60 derivatives with equally efficient electron acceptors, the preferred way to improve the solar cell efficiency is through the choice of the polymer [13,14], or by controlling the morphology of the samples. It also has been demonstrated that an annealing step is necessary to enhance the device performance [15,16]. Much effort has been put in understanding the device physics and optimizing the efficiency of the OPV cells [17-22]. Another problem to be overcome in the OPV devices is the rapid degradation, mostly due to UV light exposure [23].

One of the options explored for optimizing the performance of OPV devices is the use of Luminescent Down-Shifting (LDS) optical filters. Although LDS materials have been widely used for improvements in photovoltaic technologies, there are a limited number of reports that have been carried out on OPVs devices [24]. For example, Kettle et-al reported the use of [Ag(POP)(Bphen)](BF4) (denoted AgPOP) as a down-shifter of incident UV light into the visible range for PTB7-based organic solar cells, without the

need for a host polymer. In that work it was shown that the luminescent down shifting layer serves two purposes: firstly it improves the photocurrent of the OPV, and thus the efficiency through enhancement of the UV spectral response of the device. Also, the work shows that the above-mentioned LDS layer reduces the effect of UV degradation, leading to enhancements in the lifetime of the tested OPV [24].

Previous research with organic-based LDS materials for improvements in $P3HT$: $PC_{61}BM$ devices has been carried out in our group. The results are highlighted in [25,26,27]. In summary, the optical characterization of several dyes was done. The aim of this initial investigation was to use these materials as LDS filters for $P3HT$: $PC_{61}BM$. Absorbance and PL spectra (see figure 2), accompanied by the figures of merit, suggested that the properties of the dyes should be further improved for practical applications. There are many parameters that can be adjusted for tuning the optical properties of the dyes. In [25] and [27], for example, the optimization of the optical properties was carried out by mixing the different dyes with different concentrations. But this is not the only way to proceed. It was also reported that the optical properties of single LDS films can be properly adjusted by changing the concentration of the host matrix solution and the concentration of the dye [26].
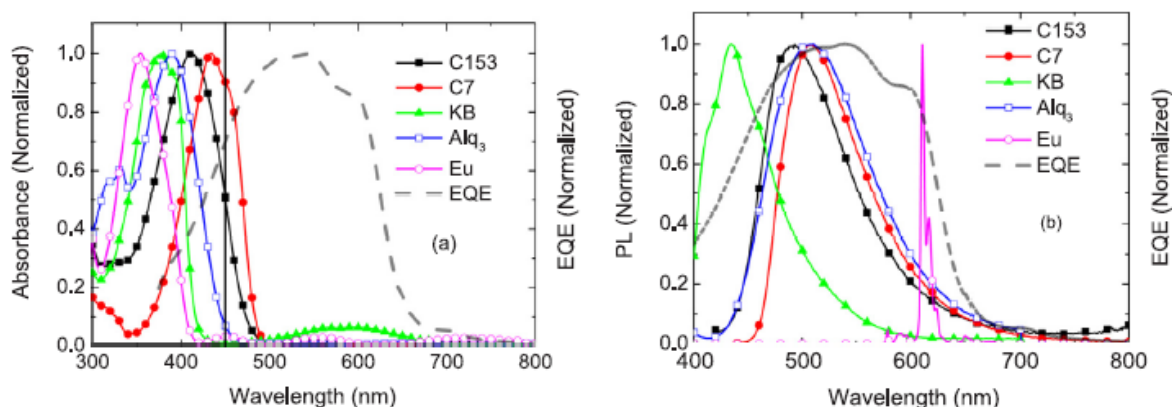
Figure 2 – Absorbance (a) and PL (b) spectra of some of the LDS materials investigated at UEL, with the External Quantum Efficiency (EQE) curve of the device (dashed line) [28].

A very interesting result found in the previous investigations is the fact that, when studying the degradation of the single LDS materials, Kremer Blue and Coumarin 7 were the films that showed better robustness upon solar exposure, as seen in figure 3. Also, the PL spectrum of Kb is overlapped with the absorbance spectrum of C7 (figure 2), suggesting that the mixture of these dyes could exhibit better properties as LDS filter when considering the probability of resonant energy transfer between the molecules.
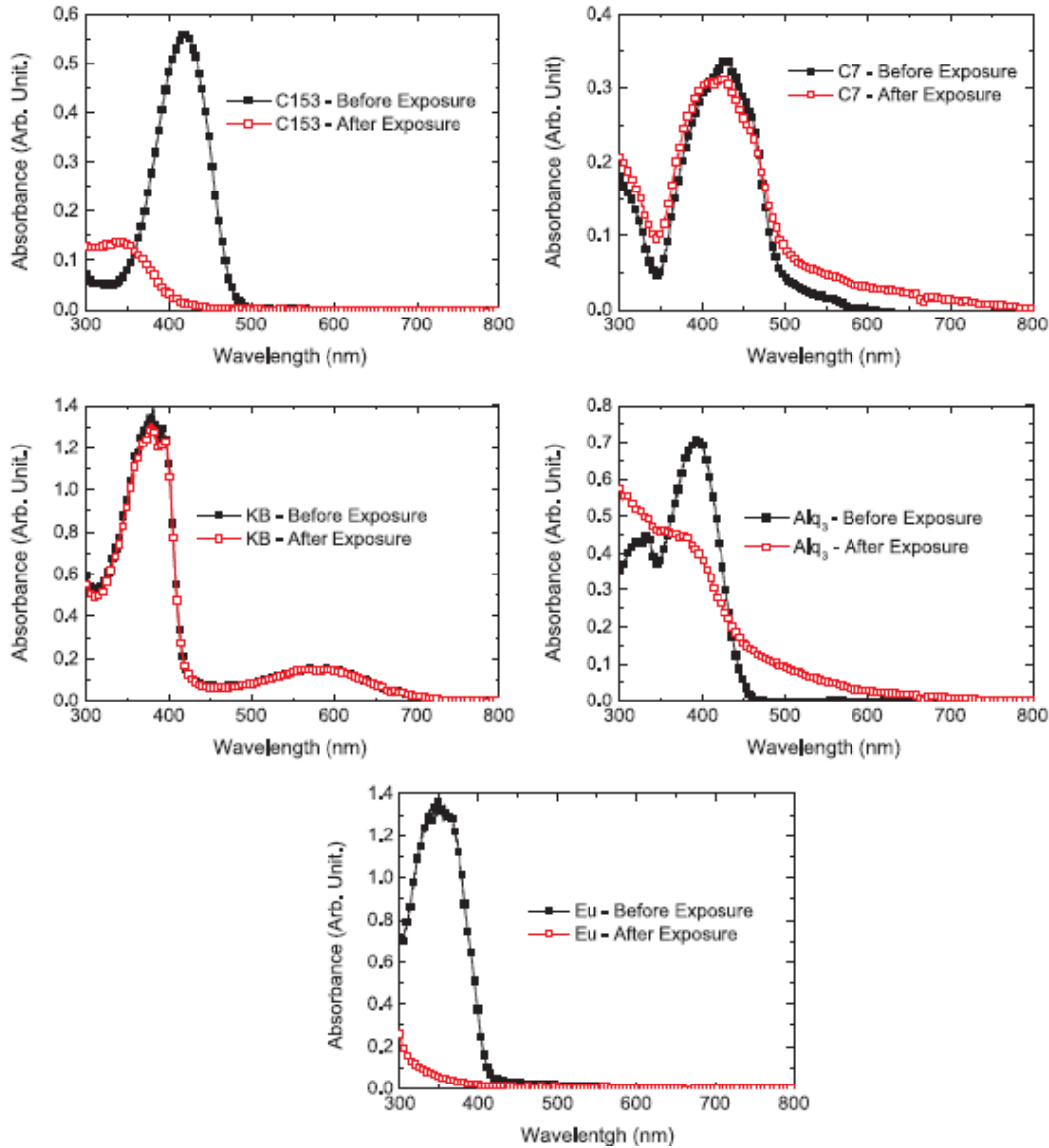
Figure 3 – Comparison between absorbance spectra of the samples, before and after the solar exposure using 1000 mW/cm^2 light intensity, according to the AM1.5G standard [28].

The possibility of using Kb-C7 blends as LDS filters for improvements in the $P3HT : PC_{61}BM$ device is explored in this work. A theoretical introduction with the concepts that will be used in this discussion is presented in chapter 2. In the chapter 3, the experimental procedure used for the synthesis of the LDS films and photovoltaic devices is given. Also, a brief theoretical description of the optical characterization techniques, as well as the conditions in which the experiments of this work were carried out are given. The simulations performed using the Rothemund model are also described at the end of this chapter. The main results are presented in chapter 4. This includes the absorbance and photoluminescence spectra of the different samples, as well as the photoluminescence quantum yield (PLQY). The EQE predictions given by the Rothemund model are given for the samples with higher values of PLQY. Decay time measurements showcasting the

energy transfer are also presented. Finally, the electrical characterization of devices, with and without LDS filters, is reported. Chapter 5 summarizes the conclusions and the forthcoming research.

1.2 Main objective

The main objective of this work is to produce LDS films of Kb-C7 useful for enhancements in the performance of the P3HT:PC61BM organic photovoltaic device.

1.3 Specific objectives

To fabricate Kb-C7 samples with different dyes concentration.

To characterize and adjust the optical properties of the different Kb-C7 films, before use them in P3HT:PC61BM devices.

To simulate the EQE curve of P3HT:PC61BM devices using the different Kb-C7 LDS filters.

To measure the I-V characteristic curve and realize any positive increment in the photo-generated current of the device by using the proper Kb-C7 film.

2 Theory

2.1 Optical properties of materials

The optical properties of a material is closely related to its electronic band structure. The electronic band structure is the amount of energy that an electron may have or not within a solid. The set of allowed energies are known as bands, while the range of prohibited energies is known as band gaps or forbidden bands. The existence of energy bands is due to the binding of two or more electrons of similar atoms. While electrons of single atoms have discrete, well-defined energy levels, when two or more atoms join together to form a molecule, their atomic orbitals overlap. Because of the Pauli exclusion principle, it is not possible for two electrons to have the same quantum numbers in a molecule. So if two identical atoms combine to form a diatomic molecule, each atomic orbital splits into two molecular orbitals of different energy, allowing the electrons in the former atomic orbitals to occupy the new orbital structure without any having the same energy. In a crystal lattice where the number of electrons are of the same order of magnitude of Avogadro's number, the number of orbitals is very large and the splitting of the orbitals make them very closely spaced in energy (of the order of 10^{-22} eV) [29]. The energy of adjacent levels is so close together that they can be considered as a continuum. That continuum of energy is the so-called band.

Electrons being quantum particles with spin $1/2$ are described by the Fermi-Dirac distribution:

$$f(\epsilon) = \frac{1}{e^{(\epsilon-\mu)/KT} + 1},\tag{2.1}$$

where T is the absolute temperature and K is the Boltzmann's constant. ϵ is an energy state occupied at thermodynamic equilibrium. μ is the Fermi level, defined as an energy level, at thermodynamic equilibrium, that has 50% probability of being occupied at any given time. For intrinsic semiconductors, the Fermi level is used to describe two important regions within the energy levels. The conduction band is the energy band located above the Fermi level, while the valence band is the energy band located below the Fermi level. The region between the maximum energy level of the valence band and the minimum energy level of the conduction band is a forbidden region in which no electron can exist. This region is known as the band gap (see figure 4).
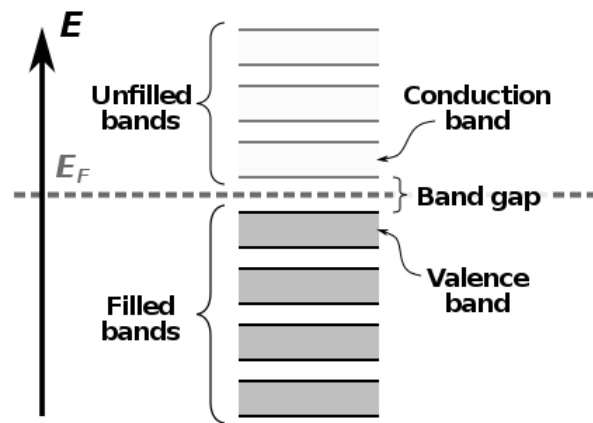
Figure 4 – Electronic band structure of a crystalline solid material [30].

The optical properties displayed by most of the materials are related to the interaction of electrons in energy bands with photons. When an atom absorbs a photon of light of correct wavelength, its electrons undergo a transition to a higher energy level. In many cases, we can think of one electron in the atom absorbing the photon and being excited. The electron will only absorb the photon if the energy of the photon matches that of the energy difference between the initial and final electronic energy levels. When this occurs, the electrons in higher energy levels will sooner or later return to the ground state. This can happen in several ways. The electron may simply emit a photon of the correct wavelength randomly, some time after it has been excited. This is known as spontaneous emission. Alternatively, a second photon may come along and instead of being absorbed, may induce the electron to emit. This is known as induced or stimulated emission and plays an important role in the action of lasers. The emitted photon in this case is in phase with, and travelling in the same direction as, the photon inducing the emission; the resulting beam of light is said to be coherent. Finally, the atom may collide with another atom, losing energy in the process or giving energy to its surroundings in the form of vibrational energy. These are examples of nonradiative transitions. The different transitions are the basis of all the known optical properties [31].

2.2   Photovoltaic effect

The photovoltaic effect is the creation of electric current in a material upon light exposure. It was first observed by French physicist A Becquerel in 1839. The flow of electrons can be originated either by direct solar exposure or due to the heating caused by absorption of the light. The heating leads to increased temperature of the semiconductor material, which is accompanied by temperature gradients. These thermal gradients in turn may generate a voltage through the Seebeck effect. Whether direct excitation or thermal effects dominate the photovoltaic effect will depend on many material parameters [32].

2.2.1 Difference between photoelectric effect and photovoltaic effect

Although photoelectric effect and photovoltaic effect are closely related, they are different concepts. The main distinction is that the photoelectric effect is refered to the electron being ejected out of the material, while the photovoltaic effect implies that the excited charge carrier is still contained within the material. In either case, an electric potential (or voltage) is produced by the separation of charges, and the light has to have a sufficient energy to overcome the potential barrier for excitation. Another important difference is the fact that photovoltaic effect is characterized by the generation of excitons, electron-hole pairs that move towards different directions within the material [32].

2.3 Semiconductors

The materials used for photogenerating current in traditional Silicon solar cells are p-n semiconductors. A semiconductor material has an electrical conductivity value between that of a conductor, such as metallic golden, and an insulator, such as wood. Its resistance decreases as its temperature increases, contrary to what is observed in a metal. Its conducting properties may be altered in useful ways by the deliberate, controlled introduction of impurities (doping) into the crystal structure. A junction is created when two differently doped regions exist in the same crystal. The behaviour of charge carriers which include electrons, ions and holes at these junctions is the basis of diodes, transistors and all modern electronics. Some examples of semiconductors are silicon, germanium, gallium arsenide. After silicon, gallium arsenide is the second most common semiconductor [33] and is used in laser diodes, solar cells, microwave frequency integrated circuits and others. Silicon is a critical element for fabricating most electronic circuits.

Semiconductors are defined by their unique electric conductive behavior, somewhere between that of a conductor and an insulator [33]. The differences between these materials can be understood in terms of the quantum states for electrons, each of which may contain zero or one electron (by the Pauli exclusion principle). These states are associated with the electronic band structure of the material. Electrical conductivity arises due to the presence of electrons in states that are delocalized (extending through the material), however in order to transport electrons a state must be partially filled, containing an electron only part of the time [33]. If the state is always occupied with an electron, then it is inert, blocking the passage of other electrons via that state. The energies of these quantum states are critical, since a state is partially filled only if its energy is near the Fermi level.

High conductivity in a material comes from it having many partially filled states and much state delocalization. Metals are good electrical conductors and have many partially

filled states with energies near their Fermi level. Insulators, by contrast, have few partially filled states, their Fermi levels sit within band gaps with few energy states to occupy. An insulator can conduct electricity by increasing its temperature: heating provides energy to promote some electrons across the band gap, inducing partially filled states in both the band of states beneath the band gap (valence band) and the band of states above the band gap (conduction band). An (intrinsic) semiconductor has a band gap that is smaller than that of an insulator and at room temperature significant numbers of electrons can be excited to cross the band gap [33].

As mentioned above, one important feature of semiconductors (and some insulators, known as semi-insulators) is that their conductivity can be increased and controlled by doping with impurities and gating with electric fields. Doping and gating move either the conduction or valence band much closer to the Fermi level, and greatly increase the number of partially filled states. The doping process consists in introducing impurities into the crystal lattice of the semiconductor. The amount of impurity, or dopant, added to an intrinsic semiconductor varies its level of conductivity. Doped semiconductors are referred to as extrinsic. By adding impurity to the pure semiconductors, the electrical conductivity may be varied by factors of thousands or millions.

The materials chosen as suitable dopants depend on the atomic properties of both the dopant and the material to be doped. In general, dopants that produce the desired controlled changes are classified as either electron acceptors or donors. Semiconductors doped with donor impurities are called n-type, while those doped with acceptor impurities are known as p-type. The n and p type designations indicate which charge carrier acts as the material's majority carrier. The opposite carrier is called the minority carrier, which exists due to thermal excitation at a much lower concentration compared to the majority carrier.

The partial filling of the states at the bottom of the conduction band can be understood as adding electrons to that band. The electrons do not stay indefinitely (due to the natural thermal recombination) but they can move around for some time. The actual concentration of electrons is typically very dilute, and so (unlike in metals) it is possible to think of the electrons in the conduction band of a semiconductor as a sort of classical ideal gas, where the electrons fly around freely without being subject to the Pauli exclusion principle. In most semiconductors the conduction bands have a parabolic dispersion relation, and so these electrons respond to forces (electric field, magnetic field, etc.) much like they would in a vacuum, though with a different effective mass [33]. Because the electrons behave like an ideal gas, one may also think about conduction in very simplistic terms such as the Drude model, and introduce concepts such as electron mobility.

For partial filling at the top of the valence band, it is helpful to introduce the concept of an electron hole. Although the electrons in the valence band are always moving around, a completely full valence band is inert, not conducting any current. If an electron is taken

out of the valence band, then the trajectory that the electron would normally have taken is now missing its charge. For the purposes of electric current, this combination of the full valence band, minus the electron, can be converted into a picture of a completely empty band containing a positively charged particle that moves in the same way as the electron. Combined with the negative effective mass of the electrons at the top of the valence band, we arrive at a picture of a positively charged particle that responds to electric and magnetic fields just as a normal positively charged particle would do in vacuum, again with some positive effective mass [33]. This particle is called a hole, and the collection of holes in the valence band can again be understood in simple classical terms (as with the electrons in the conduction band).

2.4   p-n junctions

A p-n junction is a boundary or interface between two types of semiconductor materials, p-type and n-type, inside a single crystal of semiconductor. The p (positive) side contains an excess of holes, while the n (negative) side contains an excess of electrons in the outer shells of the electrically neutral atoms there. This allows electrical current to pass through the junction only in one direction. The p-n junction is created by doping, for example by ion implantation, diffusion of dopants, or by epitaxy (growing a layer of crystal doped with one type of dopant on top of a layer of crystal doped with another type of dopant). If two separate pieces of material were used, this would introduce a grain boundary between the semiconductors that would severely inhibit its utility by scattering the electrons and holes. p-n junctions are elementary building blocks of semiconductor electronic devices such as diodes, transistors, solar cells, LEDs, and integrated circuits; they are the active sites where the electronic action of the device takes place.

In a p-n junction, without an external applied voltage, an equilibrium condition is reached in which a potential difference forms across the junction. At the junction, the free electrons in the n-type are attracted to the positive holes in the p-type. They diffuse into the p-type, combine with the holes, and cancel each other out. In a similar way the positive holes in the p-type are attracted to the free electrons in the n-type. The holes diffuse into the n-type, combine with the free electrons, and cancel each other out. The positively charged, donor, dopant atoms in the n-type are part of the crystal, and cannot move. Thus, in the n-type, a region near the junction becomes positively charged. The negatively charged, acceptor, dopant atoms in the p-type are part of the crystal, and cannot move. Thus, in the p-type, a region near the junction becomes negatively charged. The result is a region near the junction that acts to repel the mobile charges away from the junction through the electric field that these charged regions create. The regions near the p-n interface lose their neutrality and most of their mobile carriers, forming the space charge region or depletion layer [33]. The electric field created by the space charge region

opposes the diffusion process for both electrons and holes (see figure 5).
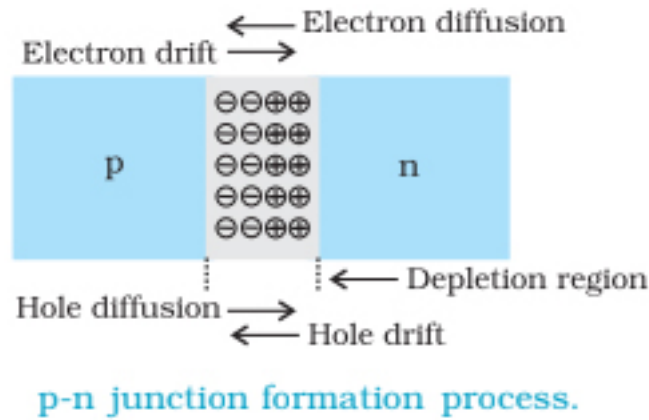
Figure 5 – Schematic of charges diffusion in p-n junctions [34].

2.5   Solar cells

The solar cell is a well known device that converts solar energy into electricity in a clean an environment-friendly way. Its working principle is based on the photovoltaic effect. Although the first cell appeared back in 1888 [35], shortly after the discovery of the photoelectric effect, the modern junction solar cells are attributed to Russell Ohl, who patented the first p-n junction solar cell in 1946 [35].
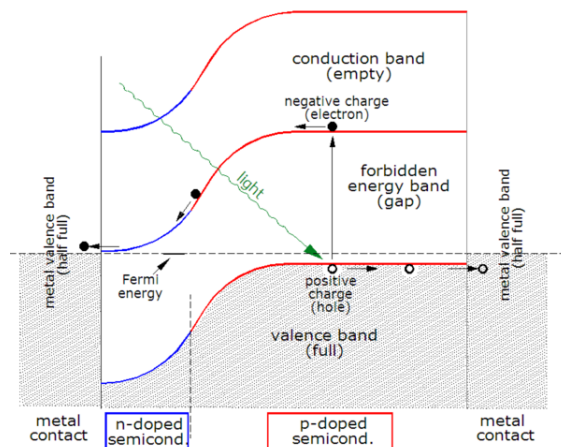
Figure 6 – Step by step of electricity production in p-n solar cells [36].

Briefly, the physical phenomena that gives place to the solar cells involves the emission of sun photons. When the photon hits a piece of a semiconductor, one of three things can happen: the photon can pass straight through the material, which is what generally happens for lower energy photons. Also, the photon can reflect off the surface, or the photon can be absorbed by the semiconductor, if the photon energy is higher than the

band gap of the compound. This generates an electron-hole pair (exciton) and sometimes heat depending on the band structure. When the photon is absorbed, its energy is given to an electron in the crystal lattice. Usually this electron is in the valence band. The energy given to the electron by the photon pushes it into the conduction band where it is free to move around within the semiconductor. The network of covalent bonds that the electron was previously a part of now has one fewer electron (or created a hole). The presence of a missing covalent bond allows the bonded electrons of neighboring atoms to move into the hole, leaving another hole behind, thus propagating holes throughout the lattice. Finally, electrons and holes are collected in the respective electrode. This cycle is continuously repeated upon solar exposure, generating a continuous flux of current. Figure 6 shows the steps needed for converting light into electricity in a p-n solar cell.

The most commonly known solar cell is made of a large area p-n junction made of silicon. Because the p-type silicon is placed in close contact with the piece of n-type silicon, a diffusion of electrons occurs from the region of high electron concentration (the n-type side of the junction) into the region of low electron concentration (p-type side of the junction). When the electrons diffuse across the p-n junction, they recombine with holes on the p-type side. However (in the absence of an external circuit) this diffusion of carriers does not go on indefinitely because charges build up on either side of the junction and create an electric field. The electric field promotes charge flow, known as drift current, that opposes and eventually balances out the diffusion of electrons and holes. This region where electrons and holes have diffused across the junction is called the depletion region because it contains practically no mobile charge carriers. It is also known as the space charge region, although space charge extends a bit further in both directions than the depletion region [35].

2.5.1 Modelling a solar cell

To understand the electronic behavior of a solar cell, it is useful to create a model which is electrically equivalent, and is based on discrete ideal electrical components whose behavior is well defined. An ideal solar cell may be modelled by a current source in parallel with a diode; in practice no solar cell is ideal, so a shunt resistance and a series resistance component are added to the model [35]. The resulting equivalent circuit of a solar cell is shown in figure 7. From the equivalent circuit, using Kirchhoff's law of nodes, we get that the current produced by the solar cell is equal to that produced by the current source, minus that which flows through the diode, minus that which flows through the shunt resistor:

$$I = I_L - I_D - I_{SH}. \tag{2.2}$$
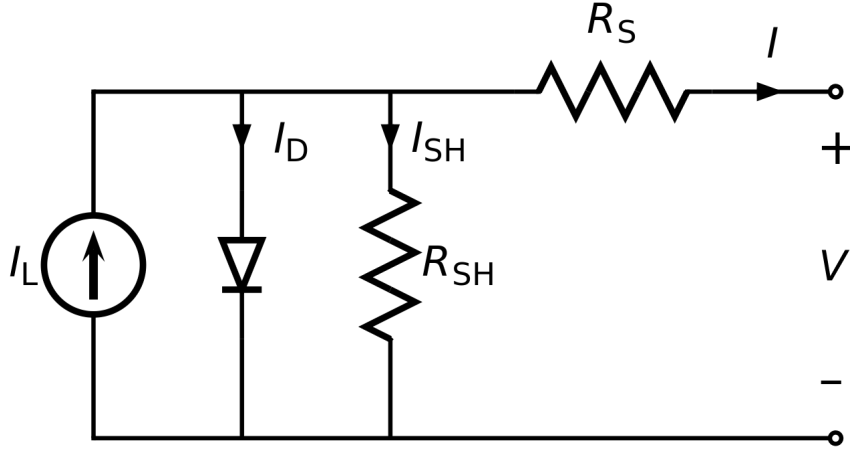
Figure 7 – Equivalent circuit of a solar cell [35].

Also, by using the other Krichhoff's law, the current through these elements is governed by the voltage across them:

$$V_j = V + IR_S, \tag{2.3}$$

where V_j is the voltage across both diode and resistor R_{SH}, V is voltage across the output terminals, I is the output current and R_S is the series resistance.

Using Ohm's law, the current diverted through the shunt resistor is:

$$I_{SH} = \frac{V_j}{R_{SH}}, \tag{2.4}$$

and using the Shockley diode equation, the current diverted through the diode is:

$$I_D = I_0(\exp^{\frac{V_j}{nV_T}} -1), \tag{2.5}$$

where I_0 is the reverse saturation current, n is the diode ideality factor (1 for an ideal diode), q is the elementary charge, k the Boltzmann's constant, T is the absolute temperature and $V_T = \frac{kT}{q}$ is the thermal voltage (0.0259 volt At 298K). Substituting equations 2.3, 2.4, 2.5 in 2.2, we get:

$$I = I_L - I_0(\exp^{\frac{V+IR_S}{nV_T}} -1) - \frac{V + IR_S}{R_{SH}}. \tag{2.6}$$

This is the characteristic equation of a solar cell, which relates solar cell parameters to the output current and voltage. Since the parameters I_0, n, R_S and R_{SH} can not be measured directly, the most common application of the characteristic equation is nonlinear regression to extract the values of these parameters on the basis of their combined effect on solar cell response. When an external load is used with the cell, its resistance can simply be added to R_S and set V to zero in order to find the current. When R_{SH} is infinite there is a solution for V for any I less than $I_L + I_0$:

$$V = nV_T \ln(\frac{I_L - I}{I_0} + 1) - IR_S. \tag{2.7}$$

When the cell is operated at open circuit, $I = 0$, the voltage across the output terminals is defined as the open circuit voltage. Assuming the shunt resistance is high enough to neglect the final term of the characteristic equation, the open circuit voltage V_{OC} is:

$$V_{OC} \approx \frac{nkT}{q} \ln(\frac{I_L}{I_0} + 1). \tag{2.8}$$

Similarly, when the cell is operated at short circuit, $V = 0$ and the current I through the terminals is defined as the short circuit current. For a high quality solar cell (low R_S and I_0, and high R_{SH}) the short circuit current I_{SC} is:

$$I_{SC} \approx I_L. \tag{2.9}$$

It is not possible to extract any power from the device when operating at either open circuit or short circuit conditions.

2.6 Solar cell parameters

When studying the performance of solar cells, it is very helpful to introduce some parameters that help to quantify how good is the device. The most used parameters are the peak power P_{max}, the short-circuit current density J_{SC}, the open circuit voltage V_{OC} and the Fill factor FF. With these parameters it is possible to calculate the conversion efficiency of the device. The open circuit voltage was already introduced in equation 2.8. It is important to emphasize that a reliable measurement of the J-V characteristic parameters, it is vital to perform the measurements under standard test conditions (STC). This means, that the total irradiance on the solar cell must be equal to 1000 W/m^2 (equal to the solar irradiance on the earth surface). Additionally, the spectrum should be similar to the AM1.5 spectrum (see [35]). Also, the temperature of the solar cell should be kept constant at 25°C.

The short-circuit current J_{SC} is the current that flows through the external circuit when the electrodes of the solar cell are short circuited. The short-circuit current of a solar cell depends on the photon flux incident on the solar cell, which is determined by the spectrum of the incident light. For standard solar cell measurements, the spectrum is standardised to the AM1.5 spectrum. The J_{SC} depends on the area of the solar cell. J_{SC} describes the maximum current that the solar cell can deliver, and it strongly depends on the optical properties of the solar cell, such as absorption in the absorber layer and reflection. The fill factor, FF, is the ratio between the maximum power ($P_{max} = i_{mpp}V_{mpp}$) generated by a solar cell and the product of V_{OC} with J_{SC}:

$$FF = \frac{J_{mpp}V_{mpp}}{J_{SC}V_{OC}}, \tag{2.10}$$

where the subscript mpp denotes the maximum power point (MPP) of the solar cell, and $J_{mpp} = \frac{i_{mpp}}{A}$, with A the area of the solar cell. To optimise the operation of PV

systems, it is very important to operate the solar cells (or PV modules) at the MPP. The photon conversion efficiency, or conversion efficiency is calculated as the ratio between the maximal generated power and the incident power. As mentioned above, solar cells are measured under the STC, where the incident light is described by the AM1.5 spectrum and has an irradiance of $I_{in} = 1000W/m^2$,

$$\eta = \frac{P_{max}}{P_{in}} = \frac{i_{mpp}V_{mpp}}{I_{in}A} = \frac{J_{SC}V_{OC}FF}{I_{in}}. \tag{2.11}$$

Typical external parameters of a crystalline silicon solar cell are; $J_{SC} = 35mA/cm^2$, V_{OC} up to 0.65V and FF in the range 0.75 to 0.80. The conversion efficiency lies in the range of 17% to 18% [35].

2.7   Bulk heterojunctions and organic photovoltaics (OPV)

Traditional Silicon solar cells are made by putting together p-doped Silicon layers with n-doped layers. However, this is not the only layer that makes possible the photon conversion into electrical current. During the last years, increasing interest has been devoted in the research of organic photovoltaics (OPV), a type of photovoltaic technology that uses organic electronics, conductive organic polymers or small organic molecules, for light absorption and charge transport [35]. For solar cells, the molecules are solution-processable at high throughput and are cheap, resulting in low production costs to fabricate a large volume. Combined with the flexibility of organic molecules, organic solar cells are potentially cost-effective for photovoltaic applications. Molecular engineering (e.g. changing the length and functional group of polymers) can change the band gap, allowing for electronic tunability. The optical absorption coefficient of organic molecules is high, so a large amount of light can be absorbed with a small amount of materials, usually on the order of hundreds of nanometers. The main disadvantages associated with organic photovoltaic cells are low efficiency, low stability and low mechanical strength compared to inorganic photovoltaic cells such as silicon solar cells.

Organic solar cells can be made by single layers, bilayers or bulk heterojunctions. Single layers are made by sandwiching a layer of organic electronic materials between two metallic conductors, typically a layer of indium tin oxide (ITO) with high work function and a layer of low work function metal such as Aluminum, Magnesium or Calcium. Bilayer are made of two layers in between the conductive electrodes. The two layers have different electron affinity and ionization energies, therefore electrostatic forces are generated at the interface between the two layers. Light must create excitons in this small charged region for an efficient charge separation and collecting. The materials are chosen to make the differences large enough that these local electric fields are strong, which splits excitons much more efficiently than single layer photovoltaic cells. The layer with higher electron

affinity and ionization potential is the electron acceptor, and the other layer is the electron donor. This structure is also called a planar donor-acceptor heterojunction. Figure 8 shows a step by step diagram of electricity production in a planar heterojunction solar cell.
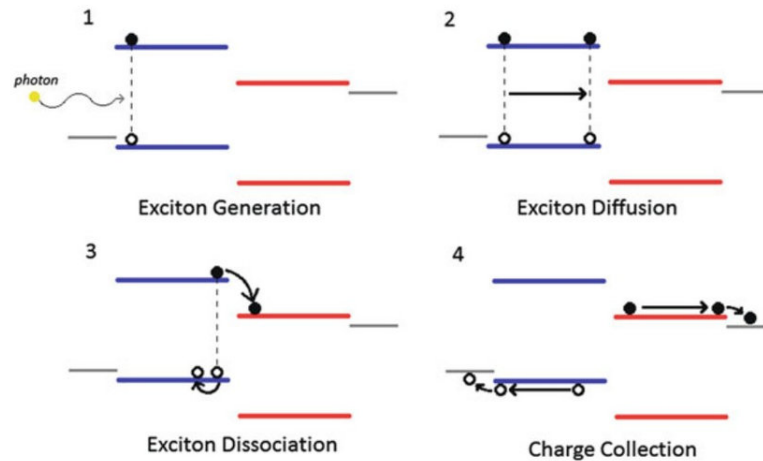
Figure 8 – Step by step of electricity production in a planar donor-acceptor heterojunction solar cell [36].

Finally, bulk heterojunctions layers consist in a nanoscale mixed blend of donor and acceptor materials. The domain sizes of this blend are on the order of nanometers, allowing for excitons with short lifetimes to reach an interface and dissociate due to the large donor-acceptor interfacial area. Bulk heterojunctions have an advantage over layered photoactive structures because they can be made thick enough for effective photon absorption without the difficult processing involved in orienting a layered structure while retaining similar level of performances. Bulk heterojunctions are most commonly created by forming a solution containing the two components, casting (e.g. drop casting and spin coating) and then allowing the two phases to separate, usually with the assistance of an annealing step [35]. The two components will self-assemble into an interpenetrating network connecting the two electrodes. Figure 9 shows a schematic of these type of solar cells.
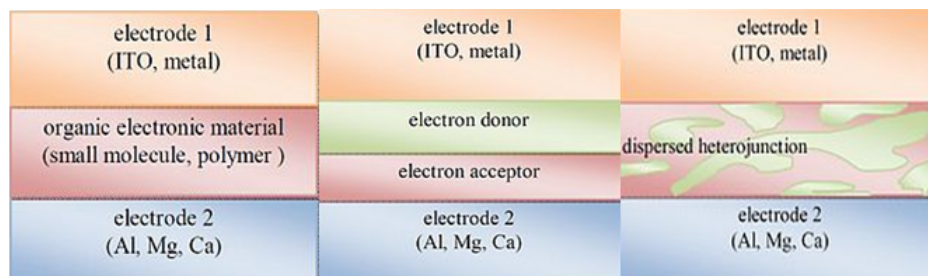
Figure 9 – Sketch of a single layer organic solar cell (left), bilayer organic solar cell (middle) and bulk heterojunction solar cell (right). Figure adapted from [37].

2.8   Reflection, refraction, absorption, and optical density

When a beam of light hits an object, there are three possible pathways for the beam: the beam can be reflected, refracted through the material or can be absorbed. Reflection of light is either specular (mirror-like) or diffuse (retaining the energy, but losing the image) depending on the nature of the interface [38]. The well known Snell's law:

$$\theta_i = \theta_r \tag{2.12}$$

states that the angle of incidence is equal to the angle of reflection. The refraction of light consists in the change of direction of the wave when it changes the medium of propagation. It is quantified by the refractive index:

$$n = \frac{c}{v}, \tag{2.13}$$

where c is the velocity of light in vacuum and v the velocity of light in the medium.
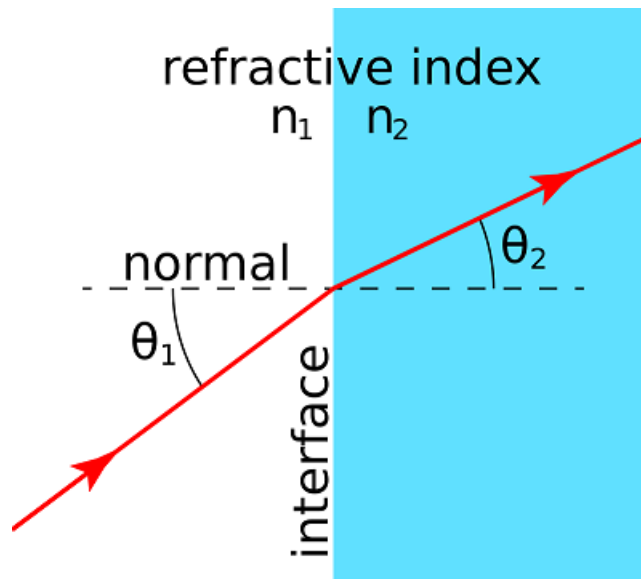
Figure 10 – Refraction of light.

As described by the second Snell's law,

$$n_1 \sin \theta_1 = n_2 \sin \theta_2, \tag{2.14}$$

the refractive index determines how much the path of light is bent in a given media.

Returning back to the absorption, there is a related concept known as transmittance. The transmittance is the fraction of incident electromagnetic power respect to the light intensity transmitted through the sample. Mathematically it is described by the equation:

$$T = \frac{\Phi_e^t}{\Phi_e^i}, \tag{2.15}$$

where Φ_e^t is the radiant flux transmitted by the surface of the material and Φ_e^i is the radiant flux received by that surface. Absorbance and transmittance are related through the Beer–Lambert law:

$$T = \frac{\Phi_e^t}{\Phi_e^i} = e^{-\tau} = 10^{-A}, \tag{2.16}$$

where τ is the optical depth and A the absorbance. The absorbance is often confused with the optical density, the latter being a measurement of a refractive medium ability to delay the transmission of light. It measures the speed of light through a substance, while the absorbance measures the ability of a refractive medium to absorb light. Where optical density measures the speed of light passing through a medium, absorbance measures how much light is lost over the course of light's passage through the given medium. Optical density also takes the scattering, or refraction, of light into consideration where absorbance does not [38].

2.9   Photoluminescence

The photoluminescence is the emission of light from any form of matter after the absorption of photons. It occurs after photons excite electrons to a higher energy level in an atom or molecule [39]. Following excitation, various relaxation processes typically occur in which other photons are re-radiated.

2.9.1   Photoluminescence quantum yield (PLQY)

The photoluminescence quantum yield (PLQY) is the ratio of the number of photons emmited per photons absorbed by the sample:

$$PLQY = \frac{\#photonsemitted}{\#photonsabsorbed}. \tag{2.17}$$

2.10   Luminescent down-shifting (LDS) effect

The luminescent down-shifting effect consist in the absorption of higher energy photons and conversion into lower energy photons. This effect allows absorbing light with a wavelength near the UV part of the spectrum, which is harmful to devices, specially organic devices, and that light is then re-emitted in a region of the spectrum that is closer to the maximum external quantum efficiency (EQE) of the device. The external quantum efficiency is the ratio of the number of charge carriers generated by the solar cell to the number of photons of a given energy hitting on the solar cell from outside. The EQE is measured as a function of the incident wavelength. Figure 11 shows the schematic effect of using LDS materials in photovoltaic devices.
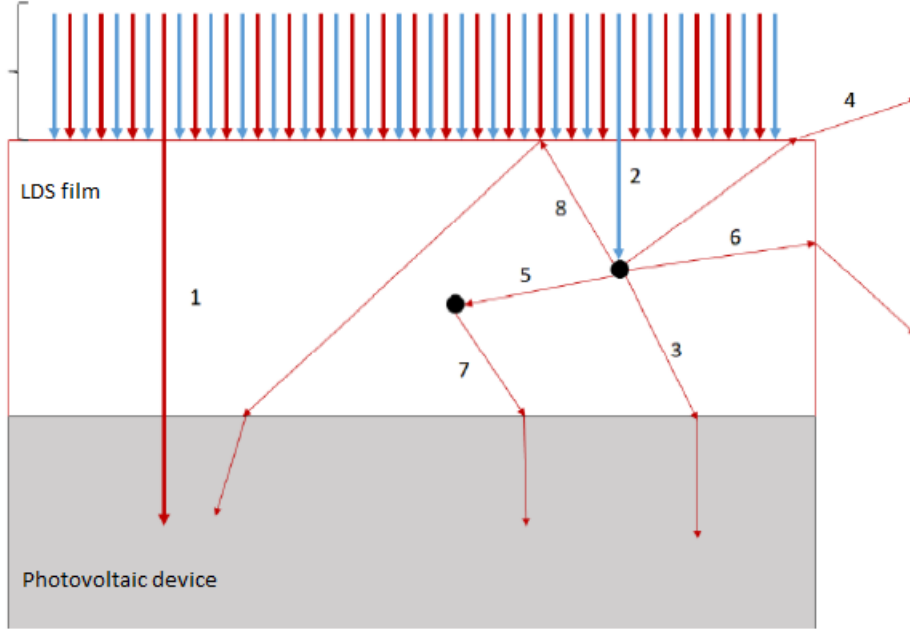
Figure 11 – Radiation with lower energy (red) passes through the LDS filter. Higher
energy radiation (blue) is absorbed by the LDS material (represented by dots),
which later emits that radiation in lower energies in different directions [28].

2.11   Figures of merit

In order to quantify the effect of LDS materials in photovoltaic devices, some figures
of merit are calculated. The most important are [28]:

2.11.1   UV Coverage (UV)

is defined as the fraction of incident light, within the UV region (300-400nm), which
is absorbed by the LDS layer and prevented from reaching the solar cell. Is calculated by:

$$UV = \frac{\int_{300nm}^{400nm}(1 - T(\lambda))AM1.5g(\lambda)d\lambda}{\int_{300nm}^{400nm}AM1.5g(\lambda)d\lambda}, \tag{2.18}$$

T being the trannsmittance of the sample.

2.11.2   Absorption spectral matching (ASM)

The absorption spectral matching (ASM) measures how well the LDS layer absorbs
photons which are not used by the solar cell. It is given by the expression:

$$ASM = \frac{\int_{300nm}^{\lambda max(EQE)}(1 - T(\lambda))\phi(\lambda)d\lambda}{\int_{300nm}^{\lambda max(EQE)}\phi(\lambda)d\lambda}, \tag{2.19}$$

where $\phi(\lambda)$ is defined as $\phi(\lambda) = AM1.5g(\lambda)[1 - EQE(\lambda)]$.

2.11.3 Parasitic absorption

The Parasitic absorption (PA) measures the absorption in the region where the solar cell performs well and should be minimized. It is calculated using the formula:

$$PA = \frac{\int_{300nm}^{900nm}(1 - T(\lambda))\Theta(\lambda)d\lambda}{\int_{300nm}^{900nm}\Theta(\lambda)d\lambda}, \tag{2.20}$$

with $\Theta(\lambda) = AM1.5g(\lambda)EQE(\lambda)$.

2.11.4 Emission spectral matching (ESM)

Emission Spectral Matching (ESM) is the measurement of how well the photoluminescence of the LDS material matches with the EQE of the solar cell. The calculation of this figure of merit is done by using:

$$ESM = \frac{\int_{30nm}^{900nm} Em(\lambda)EQE(\lambda)d\lambda}{max[EQE(\lambda)]\int_{30nm}^{900nm} Em(\lambda)d\lambda}. \tag{2.21}$$

2.11.5 Radiative overlap (RO)

the radiative overlap (RO) measures the overlap between the absorption and photoluminescence spectra. This figure of merit should be minimized. It is given by the expression:

$$RO = \frac{\int_{30nm}^{900nm}(1 - T(\lambda))Em(\lambda)d\lambda}{\int_{30nm}^{900nm} Em(\lambda)d\lambda}. \tag{2.22}$$

2.12 Rothemund model

The effect of LDS materials in the EQE of a photovoltaic device can be predicted by using different models available in the literature [40]. In the present work, we opt to use the Rothemund model, because of its simplicity. When using this model, low-cost calculations are carried out, and the results are very reliable when compared to the experimental data [41]. The characteristic equation of the model is:

$$EQE_{LDS} = EQE_{ref}T(\lambda) + n(1 - T(\lambda)) * ESM * PLQY. \tag{2.23}$$

EQE_{ref} is the measured EQE curve of the device, without filter, T is the transmittance for the LDS material, ESM is the emission spectral matching and PLQY is the photoluminescence quantum yield. n is known as the loss factor.

2.13 Fluorescence Resonance Energy Transfer (FRET)

The fluorescence resonance energy transfer, also known as Förster resonance energy transfer, is a mechanism describing energy transfer between two light sensitive molecules

[39]. A donor, initially in its electronic excited state, may transfer energy to an acceptor through nonradiative dipole–dipole coupling [39]. The efficiency of this energy transfer is inversely proportional to the sixth power of the distance between donor and acceptor, making FRET extremely sensitive to small changes in distance. The term fluorescence sometimes leads to misunderstanding about the concept. As mentioned, FRET is a non-radiative process, and thus no fluorescence emission is mediating the energy transfer.

The FRET efficiency depends on many physical parameters like the distance between the donor and the acceptor, the spectral overlap of the donor emission spectrum and the acceptor absorption spectrum, and the relative orientation of the dipole moments of the molecules. The distance dependence of the quantum yield is described by the following equation:

$$\phi = \frac{1}{1 + (r/R_0)^6}, \tag{2.24}$$

with R_0 being the Forster distance between donor and acceptor. This is the distance at which the efficiency of the transfer is 50%. The Forster distance depends on the overlap integral of the donor emission spectrum with the acceptor absorption spectrum and their mutual molecular orientation as expressed by the following equation:

$$R_0^6 = \frac{2.07}{128\pi^5 N_A} \frac{\kappa^2 Q_D}{n^4} \int F_D(\lambda)\epsilon_A(\lambda)\lambda^4 d\lambda, \tag{2.25}$$

where Q_D is the fluorescence quantum yield of the donor in the absence of the acceptor, κ^2 is the dipole orientation factor, n is the refractive index of the medium, N_A is Avogadro's number.

The energy transfer efficiency and the lifetime of donor molecules are related by the equation:

$$\phi = 1 - \frac{\tau_D'}{\tau_D}, \tag{2.26}$$

where τ_D' and τ_D are the lifetime of donor molecules in presence and absence of the acceptor molecules, respectively.

2.14   Design of experiments (DOE)

The design of experiments is a methodology based on statistics useful in multi-variables analyses of data. It provides a tool to plan experiments and avoid unnecessary repetitions [42]. For the factorial experiments, at least two different levels of the same variable are needed. In general, a design of experiments has n^k experiments, where n represent the number of levels, i.e. the different values of a given parameter, and k represents the number of factors, or parameters, varied during the experiments. In 2-fold factorial experiments, the lowest level is represented by a - sign, while the highest level is represented by a + sign. The elements are usually located in a table, together with the mean value of the response variable in each level.

The contrast matrix is a rectangular array that allows us to calculate the effects of the factors and their interactions. For a 2^2 design, it is given by:

$$X = \begin{bmatrix} + & - & - & + \\ + & + & - & - \\ + & - & + & - \\ + & + & + & + \end{bmatrix}.$$ (2.27)

In general, the first column of the constrast matrix has a $+$ sign in all its elements, while the other columns has alternating values of - and $+$, representing the variation of the levels in each factor. In the previous matrix, the first column is related to the mean value of the response for all the levels, the second column is related to the effect of the first factor (C), the third column is related to the effect of second factor (D), and the fourth column is related to the eect of the interaction of the two factors (CD). The effect vector Y is given by the mean value of the response in each level:

$$Y = \begin{bmatrix} \frac{Y_{11}+Y_{12}}{2} \\ \frac{Y_{21}+Y_{22}}{2} \\ \frac{Y_{31}+Y_{32}}{2} \\ \frac{Y_{41}+Y_{42}}{2} \end{bmatrix}.$$ (2.28)

The final effect elements will be given by:

$$M = X^t Y = \begin{bmatrix} \frac{Y_{11}+Y_{12}+Y_{21}+Y_{22}+Y_{31}+Y_{32}+Y_{41}+Y_{42}}{2} \\ \frac{Y_{21}+Y_{22}+Y_{41}+Y_{42}-(Y_{11}+Y_{12}+Y_{31}+Y_{32})}{2} \\ \frac{Y_{31}+Y_{32}+Y_{41}+Y_{42}-(Y_{11}+Y_{12}+Y_{21}+Y_{22})}{2} \\ \frac{Y_{11}+Y_{12}+Y_{41}+Y_{42}-(Y_{21}+Y_{22}+Y_{31}+Y_{32})}{2} \end{bmatrix}.$$ (2.29)

The mean value of the response is given by the first element divided by four (M11/4), while the effects of the factors and their interactions are calculated by dividing the other elements of the vector by two.

The variance is given by:

$$s^2 = \frac{\sum_i (x_i - \bar{x})^2}{n - 1},$$ (2.30)

where $\bar{x}$ is the mean value of the response and n is the number of responses of each level. The typical error associated to an specific effect is given by:

$$s(effect) = \sqrt{\frac{s^2}{2}}.$$ (2.31)

with this typical error, we can use the t-student distribution with m degrees of freedom and 95% of confidence (t_m) and realize which factors are significant in the design of experiment. The significant factors are those whose absolute value is higher than $t_m \times s(effect)$

3 Experimental methods

3.1 Fabrication of the samples

The fabrication of the materials used in this work involved two different steps. First, LDS films were fabricated in order to carry out the optical characterization. After calculating the figures of merit and optimize the samples, we proceed to apply the optimal film to a $P3HT : PC_{61}BM$ device, in order to test the performance improvement of the device caused by the LDS layer.

3.1.1 Fabrication of LDS films

The LDS films used in the present work are mixtures of Kremer Blue (Kb) and Coumarin 7 (C7). The next figure shows the chemical composition of these dyes.
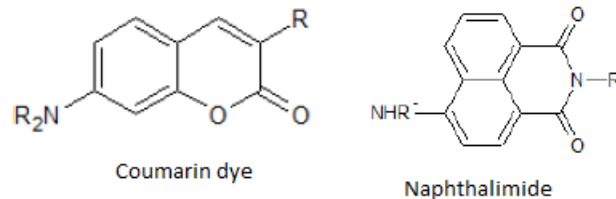
Figure 12 – Chemical structure of Coumarin and Kremer Blue (Naphthalimide) dyes [28].

A solution of Poly-methyl-methacrylate (PMMA), commercially known as acrylic, was used as polymeric matrix for the powder dyes. The PMMA was dissolved in dichlorobenzene, with different concentrations varying from 0.25mg/mL to 5mg/mL. The solutions were stirred in a magnetic plate for 24h, in order to guarantee homogeneous solutions. Powder samples of Kb and C7, obtained from Kremer and Sigma Aldrich respectively, were weighted in a digital balance. Samples with different mass-mass concentration were dispersed into the PMMA solutions. Dyes solutions were stirred for 24h in the magnetic plate. Quartz substrates, previously cleaned with deionized water, acetone and isopropilic alcohol, were used to drop cast the solutions. All the LDS films were casted using $100\mu L$ of solution.

3.1.2 Fabrication of P3HT:PC61BM devices

Glass substrates with an Indium Tin Oxide (ITO) thin film were used for the synthesis of OPVs. The substrates were cleaned using the same procedure used for cleaning the

quartz substrates, and 5min ultrasound baths were applying between each cleaning step. After that, a conductor film of poly(3,4-ethylenedioxythiophene) polystyrene sulfonate (PEDOT:PSS) was deposited by spin coating. The substrate was rotated with a velocity of 4500 rpm for 30 s. Thermal annealing at $60°C$ for 1 hour was done, in order to remove potential residuals from the solvent. The devices were fabricated at ambient conditions. The active layer of $P3HT : PC_{61}BM$, in a proportion of 17: 13 in mass, was dissolved in chlorobenzene, resulting in a solution of 30 mg/mL of concentration. The solution was stirred for 24h and then it was deposited by sping coating in the substrates. A rotation of 1500 rpm for 60 s was used. After that, the samples were heated at $150°C$ for half an hour. Aluminum electrodes were deposited by thermal evaporation. All the reactants were obtained from Sigma Aldrich. Figure 13 shows the type of devices used in this work.
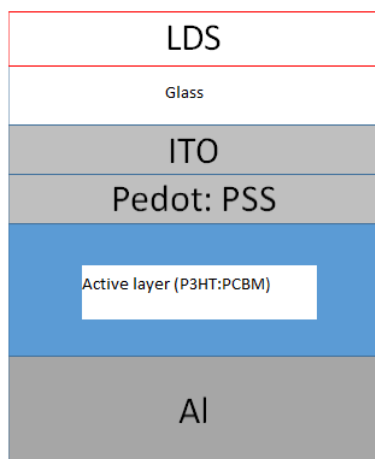
Figure 13 – Photovoltaic devices used in this work [28].

3.2   Characterization

3.2.1   Absorbance

The absorbance of LDS films was measured by means of a UV-3600 Shimadzu spectrophotometer [43] with a resolution of 0.1nm over the range 185 to 3300nm. The working principle of a spectrophotometer is based on the Beer-Lambert relation (see 2.15 and 2.16). Two beams of light are used for the absorbance measurement. First, the intensity of a light beam is measured without the sample set. Then the sample is set in the path of the measurement light beam, and the intensity of the light beam after it passes through the sample is measured. Figure 14 illustrates the measurement process using the spectrophotometer.
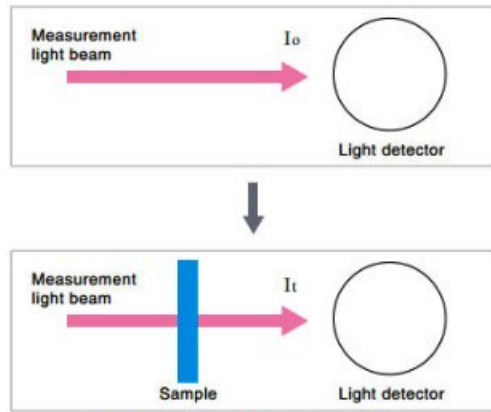
Figure 14 – Measuring process using a spectrophotometer. First, beam intensity is measured without the sample, and after that the same measurement is carried out, setting the sample in front of the light beam [43].

The experimental setup consists in a light source, a monochromer, a sample compartment, and a detector.
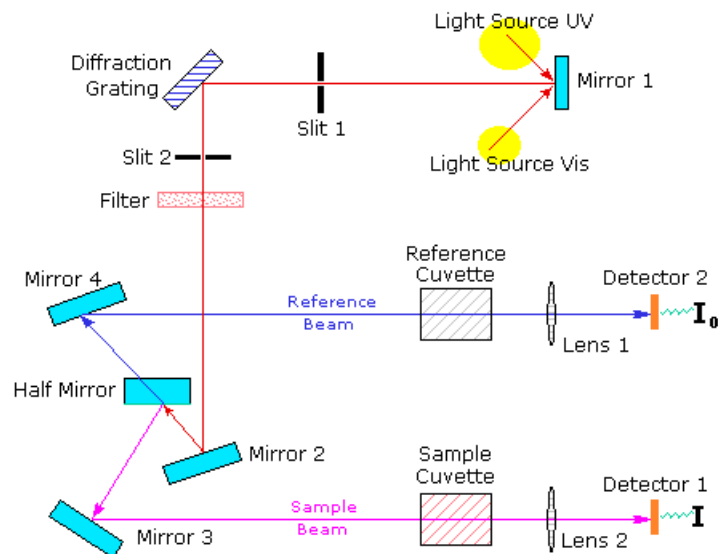
Figure 15 – Components of a spectrophotometer [43].

3.2.2   Photoluminescence and quantum yield

Photoluminescence measurements were carried out with an Ocean Optics USB4000 minispectrometer and a 375 nm diode laser as excitation source. For the PLQY measurements, an integrating sphere (5 inches diameter) was used. The well known three-steps measurement using the integrating sphere was used to determine both the PL spectra and the photoluminescence quantum yield (PLQY). The procedure of measuring the PLQY of a solid sample using an integrating sphere is described in [44]. As seen in figure 16, the three measurements needed are: a) the sphere is empty, b) the sample is inside the sphere,

but the laser beam is directed to the sphere wall and c) the sample is inside the sphere and the laser beam is directed to the sample. When measuring these PL profiles, there will be a peak at the excitation wavelength and another peak related to the compound. As in experiment a) there is no sample, in that profile we will see just a peak at the excitation wavelength (see figure 17).
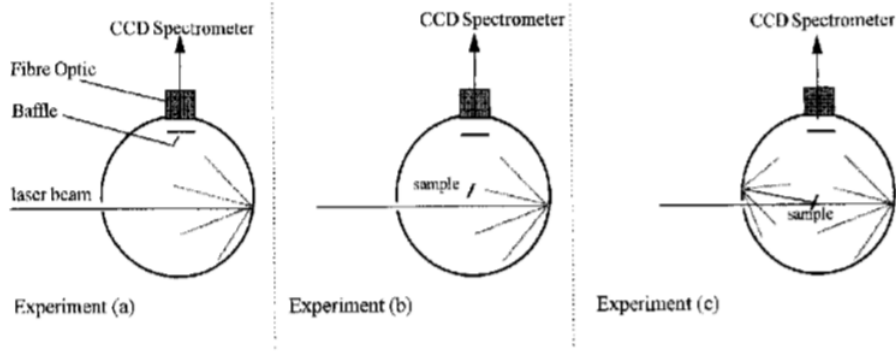
Figure 16 – 3 steps measurement of PLQY using the integrating sphere method [47].

Let's call L the area under the curve for the excitation peak, and P the area under the curve of the second peak (related to the sample). By doing some considerations and assuming that laser light scattered from different locations on the sphere interior contributes identically to the measured spectrum [44], the PLQY is given by:

$$PLQY = \frac{P_c - (1 - A)P_b}{L_a A},\tag{3.1}$$

where $A = 1 - \frac{L_c}{L_b}$ is the absorption coefficient. L_a, L_b and L_c are the area under the curve related to the excitation peak for experiments a, b and c, respectively. P_b and P_c are the area under the curve associated to the sample in experiments b and c, respectively. The profile of experiment c showing just the peak associated to the sample (P_c peak) is the PL spectra of the sample.
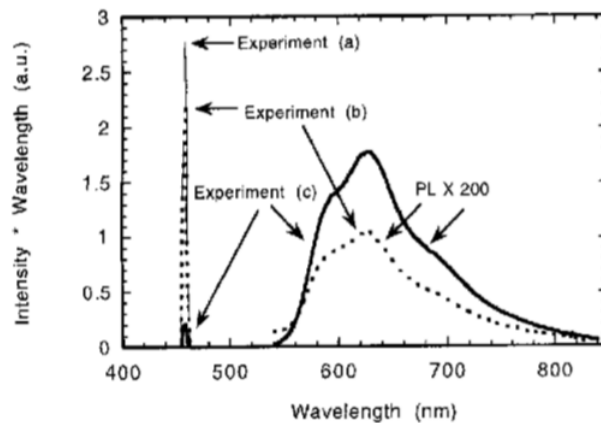
Figure 17 – PL profiles obtained with the three different configurations of the sample using the integrating sphere for PLQY measurements [44].

3.2.3 Photoluminescence decay time

Photoluminescence decay time measurements were carried out in order to verify the possible energy transfer process occurring between Kb and C7 molecules. The lifetime of different samples, with different PMMA solution and different mass-mass concentration of dyes, were measured. TRPL was done using the PicoQuant FluoTime 300 system. Various types of set-up can be used for TRPL measurements, they can be broadly divided into three categories: spectrometers, confocal microscopes or combinations of both instruments.For time-resolved experiments, the sample is excited by a pulsed laser, LED, or Xe-flash lamp. The emitted signal is detected by a detector with sensitivity in the UV/Vis or NIR spectral region. Selection of the emission wavelength can be done via either a monochromator, long pass, band pass or variable filters. For lifetime measurements, either Time-Correlated Single Photon Counting (TCSPC) or Multi-Channel Scaling (MCS) electronics are used for data acquisition [45]. The experimental set-up of a photoluminescence decay time equipment is shown in figure 18.

Figure 18 – Photoluminescence decay time set-up [45].

The experiments were carried out with an excitation wavelength of 375 nm (closer to the maximum of absorbance of Kb) with a pulsed laser and the detection wavelength were 440 nm (close to the maximum of Kb emission) and 510 nm (close to the maximum of C7 emission).

4 Results

As mentioned in the introduction, there are two possible approaches to enhance the properties of LDS organic films. One way is to optimize the properties of single LDS films, the other is to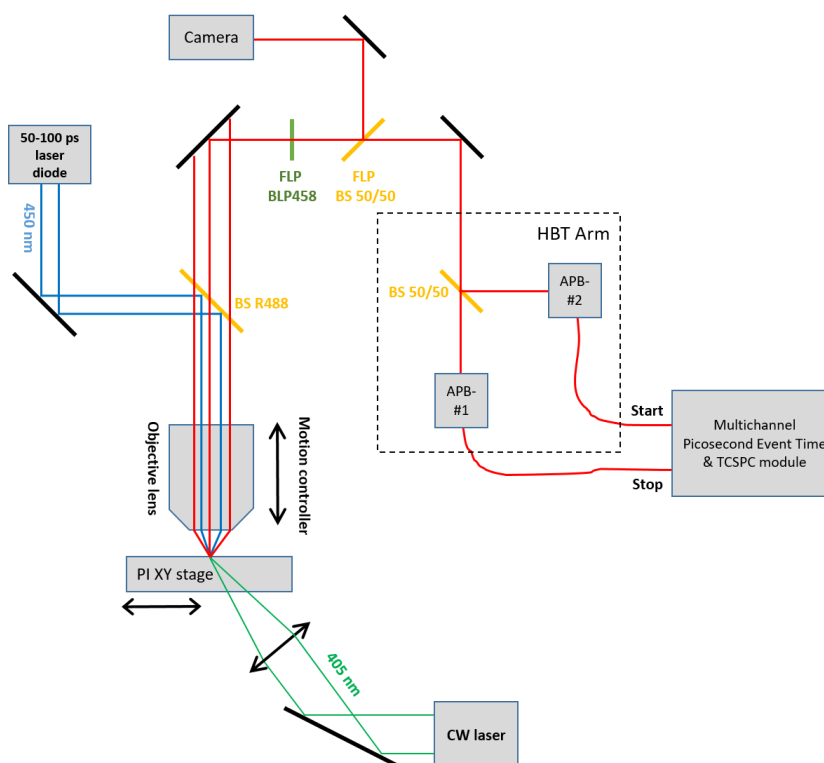 mix two different dyes and adjust the optical properties by varying the concentration of the dyes. In this work, the latter option has been explored using Kb-C7 mixtures. Before presenting the results obtained with this blend, the results of the optimization process of single Kb LDS films is presented.

The optimization process follows predictions made by using Rothemund model (eq. 2.23). According to the model, by keeping the absorbance and the ESM almost fixed, an increment in the EQE of the device is obtained by increasing the PLQY. Simulations made by Fernandes et-al [28] show that a maximum of absorption between 0.7 and 1.2 will lead to significant enhancements in the EQE of the device. The photogenerated current density J, which is proportional to the area under the curve of the EQE, is increased by using LDS filters with high PLQY value. This is precisely the result obtained by Fernandes [26]. Figure 18 shows the variation of current density for devices under Kb LDS layers with different PLQY and maximum absorption values. The graphic shows that there will only be an increase in the photocurrent density if the PLQY of the layer is greater than 60%. In addition, the gains become larger as the absorbance of the layer increases. However, there is a saturation of this gain for higher values of absorbance, which indicates that, for each PLQY value, there is an optimum absorbance value for the best performance of the Kb layer as a down-shifter. Based on these predictions, a Kb layer optimization process was performed with the aim of obtaining the highest possible PLQY value, with an absorbance maximum intensity above 0.7.
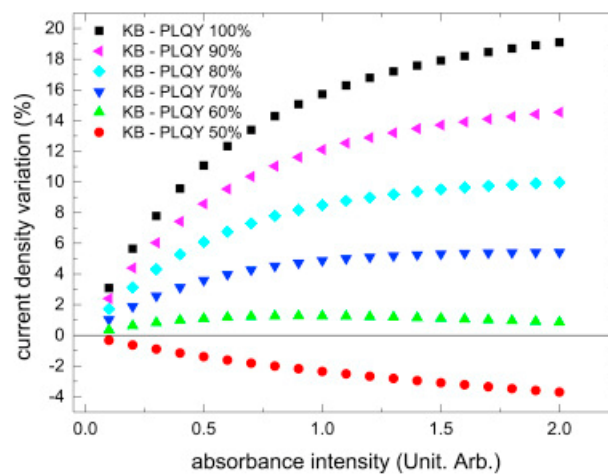
Figure 19 – Simulations of the influence of LDS (Kb) layer PLQY values on current density of P3HT: PC61BM photovoltaic devices for different absorbance maximum values [26].

The simulations based on the Rothemund model predicted an increment of 6% in the photogenerated current using the optimized Kb sample. The test carried out on 9 devices, reported an average increment of 6.7% in the photogenerated current, which is in very good agreement with the theoretical prediction. See figure 20.
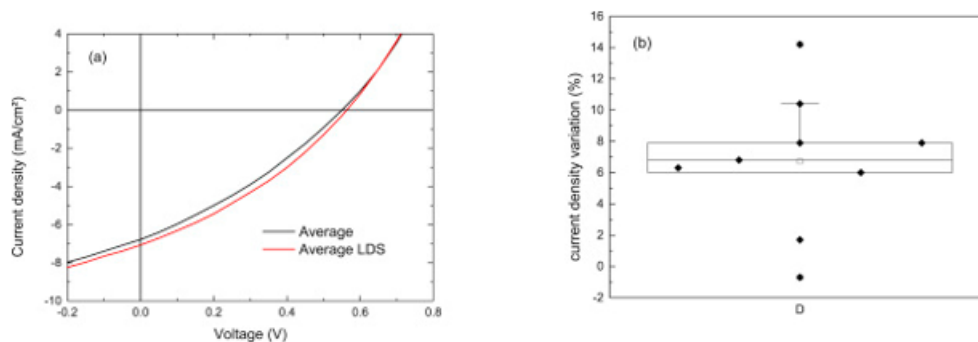
Figure 20 – a) J versus V mean curve for the nine devices analyzed before and after the application of the Kb LDS layer. b) current density variation for the nine devices tested in [26].

4.1   Absorbance, photoluminescence and PLQY

The present work aims to produce similar results using Kb-C7 mixtures. The results of the first set of experiments, consisting in the absorbance and PL spectrum of three samples, is highlighted in figure 21.

Figure 21 – Photoluminescence (rightt) and absorbance (left) spectra of $Kb_{80}C7_{20}$, $Kb_{90}C7_{10}$ and $Kb_{95}C7_5$ samples dissolved in PMMA(1.85mg/mL).

This first measurement round was carried out with the intention of knowing the effect of dyes concentration in absorbance and PLQY. The table presents the PLQY values obtained for these samples.

Table 1 – First set of experiments for Kb-C7 samples. The PMMA concentration was 1.85 mg/mL for all the samples.

Sample	PLQY
$Kb_{95}C7_5$	23.9 ±1.2
$Kb_{90}C7_{10}$	35.5 ±1.8
$Kb_{80}C7_{20}$	37.8 ±1.9

As an initial hint, the results show that increasing the content of Coumarin increases the PLQY value. It is also known that the concentration of host polymeric matrix affects the properties of the films. A second experiment was carried out to evaluate the effect of PMMA concentration in the absorption and PL of the samples. This time, $Kb_{99.5}C7_{0.5}$ samples dissolved in 0.25mg/mL and 1.85mg/mL PMMA were analysed. The spectrum are shown in figure 22.
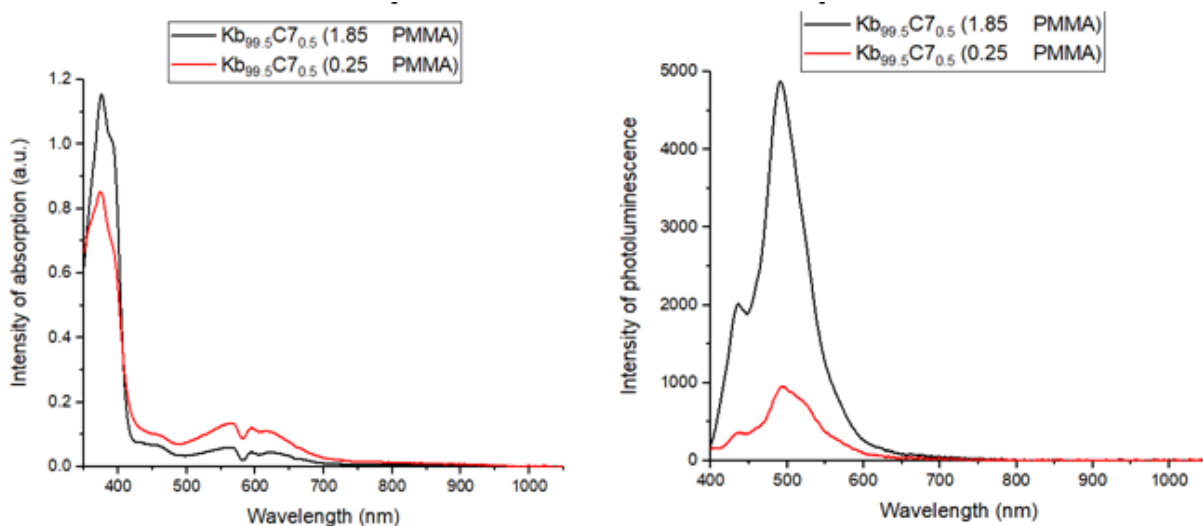
Figure 22 – Photoluminescence (right) and absorbance (left) spectra of $Kb_{99.5}C7_{0.5}$ samples dissolved in 0.25mg/mL and 1.85mg/mL PMMA.

Notice that there is a small narrow peak in the absorption spectra over the 500nm - 700nm range. The PL maximum is much higher for the sample dissolved in higher concentration of PMMA (1.85mg/mL).

Table 2 – Second set of experiments for $Kb_{99.5}C7_{0.5}$ samples.

PMMA concentration (mg/mL)	Number of repetitions	PLQY
0.25	3	4.7 ±0.6
1.85	3	24.5 ±4.0

As seen in the table 2, for a given concentration of KB-C7 (mass-mass content), PLQY is higher for higher PMMA concentrations. Although the absorbance and PL match the re-

quirements of a filter useful for enhancements of the $P3HT : PC61BM$ device (absorbing near the UV and emitting within the range of maximum EQE of the device), the PLQY values are still very low, so further samples were synthetized.

The third set of absorbance and PL measurements were carried out in two different samples with two different PMMA solutions. The absorbance and PL spectra of $Kb_{92.5}C7_{7.5}$ and $Kb_{95}C7_5$ samples dissolved in 2.15 and 3mg/mL PMMA are shown in figure 23.

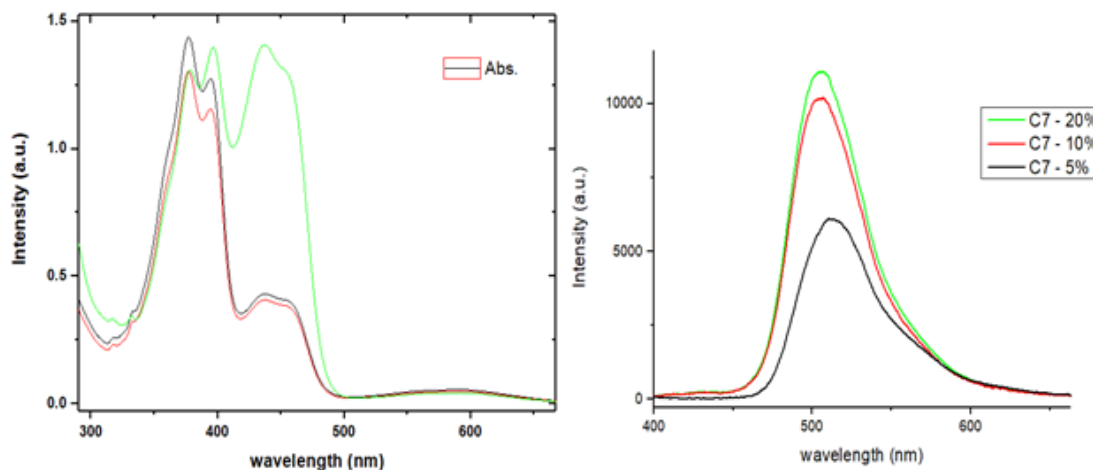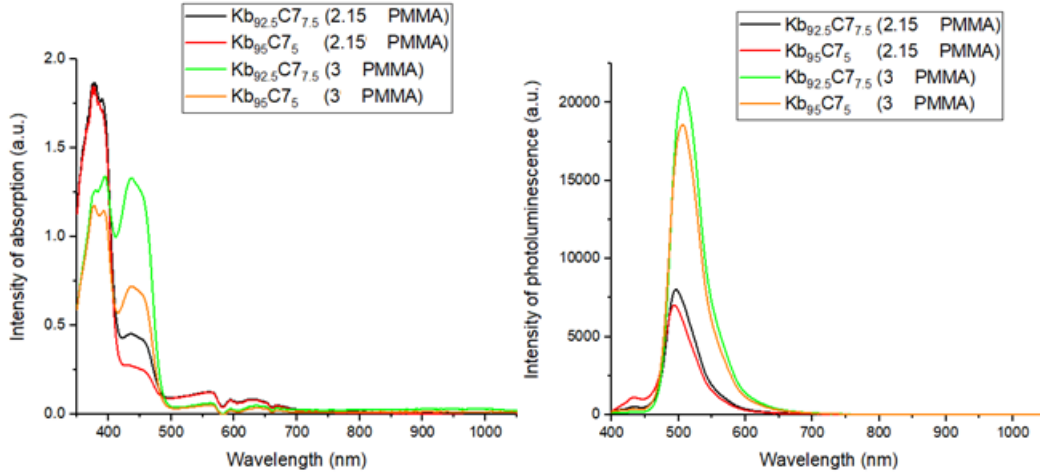Figure 23 – Photoluminescence (right) and absorbance (left) spectra of $Kb_{92.5}C7_{7.5}$ and $Kb_{95}C7_5$ samples dissolved in 2.15 and 3mg/mL PMMA.

This set of experiments were carried out using a design of experiments (DOE). For this DOE, two factors were varied: PMMA concentration and donor-acceptor proportion. For each factor, two levels were chosen and duplicate experiments were done in order to calculate the intrinsic error associated to the experiments. The table 3 shows the results of this design of experiments.

Table 3 – First design of experiments for Kb-C7 samples.

PMMA concentration	Dyes concentration	PLQY 1	PLQY 2	Mean value	variance
2.15 mg/mL (-)	$Kb_{92.5}C7_{7.5}(-)$	24.9	34.5	29.7 $\pm$6.8	46.1
3 mg/mL (+)	$Kb_{92.5}C7_{7.5}(-)$	85.4	67.1	76.3 $\pm$12.9	167.4
2.15 mg/mL (-)	$Kb_{95}C7_5(+)$	28.4	27.1	27.8 $\pm$0.9	0.8
3 mg/mL (+)	$Kb_{95}C7_5(+)$	82.3	81.8	82.1 $\pm$0.4	0.1

With the previous results, it is possible to calculate the effect of the factors and the errors associated to each factor. For this we will use the matrix formulation explained in [42].

The contrast matrix is given by:

$$X = \begin{bmatrix} + & - & - & + \\ + & + & - & - \\ + & - & + & - \\ + & + & + & + \end{bmatrix}, \tag{4.1}$$

where the first column corresponds to the mean value of the answer for all the measurements (PLQY), the second column is related to the effect of PMMA concentration (C), the third column is related to the effect of dyes concentration (D), and the fourth column is related to the effect of the interaction of these two factors (CD). With the mean values for each level, the effect vector is given by:

$$Y = \begin{bmatrix} 29.7 \\ 76.3 \\ 27.8 \\ 82.1 \end{bmatrix}. \tag{4.2}$$

The final effect elements will be given by:

$$M = X^t Y = \begin{bmatrix} 215.9 \\ 100.9 \\ 3.9 \\ 7.7 \end{bmatrix}. \tag{4.3}$$

The mean value of the PLQY is given by the first element divided by four ($PLQY = 54.975$), and the effects of the factors (PMMA concentration C and dyes concentration D) and their interactions are calculated by dividing the other elements of the vector by two:

$$C = \frac{100.9}{2} = 50.45, \tag{4.4}$$

$$D = \frac{3.9}{2} = 1.95 \tag{4.5}$$

and

$$CD = \frac{7.7}{2} = 3.85 \tag{4.6}$$

The typical error is given by the square root of the variance mean value:

$$s = \sqrt{s^2} = \sqrt{\frac{46.1 + 167.4 + 0.8 + 0.1}{4}} = \sqrt{53.6} = 7.321 \tag{4.7}$$

The typical error associated to an specific effect is given by:

$$s(effect) = \sqrt{\frac{s^2}{2}} = 5.176 \tag{4.8}$$

with this typical error, we can use the t-student distribution with four degrees of freedom and 95% of confidence ($t_4 = 2.776$) and realize which factor are significant in this design of experiment. The significant factors are those whose absolute value is higher than $t_4 \times s(effect) = 2.776 \times 5.176 = 14.371$. Thus for this design of experiments the only significant factor is the PMMA concentration C.

In these results something very curious happens. The samples dissolved in 3mg/mL PMMA have PLQY values higher than 70, which are acceptable values according to the Rothemund model. However, notice that the PLQY of the sample $Kb_{92.5}C7_{7.5}$ has a deviation of 9.15. When measuring PLQY values, a deviation lower than 5% is expected, according to the scientific literature [44]. This result should be either discarded or verified. For that reason, another design of experiments with $Kb_{92.5}C7_{7.5}$ samples was carried out. This time, 3 samples were fabricated and the number of repetitions of PLQY measurements was increased by 3. The samples were also dissolved in 5mg/mL PMMA, in order to verify which sample exhibits higher PLQY value. The only factor varying in this design of experiments is the PMMA concentration. These results are showcasted in figure 24. The following table summarizes the results of this design of experiments:

Table 4 – Second design of experiments for Kb-C7 samples.

PMMA concentration	1	2	3	4	5	6	Mean value	variance
3mg/mL(-)	92.3	88	97.8	94.6	93.2	95.9	93.6 ±2.9	40.6
5mg/mL(+)	79.8	76.3	75	79.5	77.7	84.8	78.9 ±3.5	59.9

Using the same procedure described for the previous design of experiment, we realize that the mean response of this design (PLQY) is equal to 86.3% and the effect of PMMA concentration is -14.7. The variance is given by:

$$s^2 = \frac{40.6 + 59.9}{2} = 50.25 \tag{4.9}$$

and the error associated to the change of PMMA concentration is given by:

$$s(effect) = \sqrt{\frac{s^2}{2}} = 5.012 \tag{4.10}$$

This time we have 10 degrees of freedom (12 measurements in 2 different levels), thus the critical value of t-student distribution with 10 degrees of freedom $t_{10} = 2.228$ allows us to realize whether the factor is significant or not. The significance is given by the critical point times the error of the effect (11.667), and because the absolute value of the concentration effect (14.7) is higher than this value, it is concluded that indeed the PMMA concentration is a significant effect.
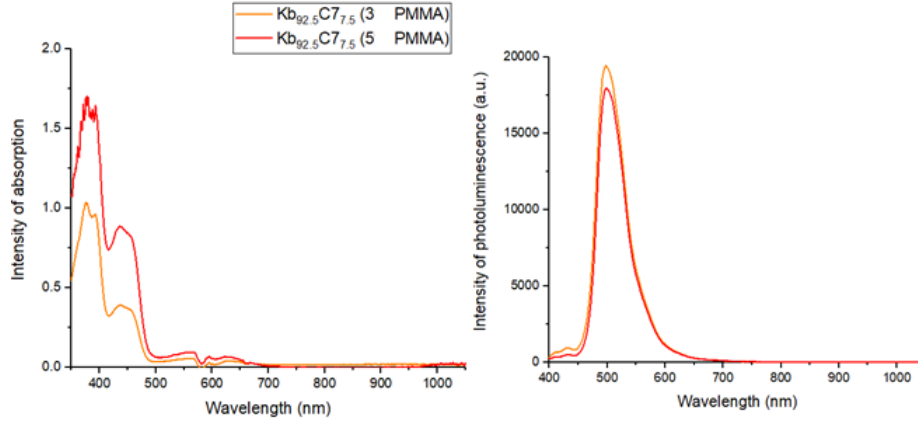
Figure 24 – Photoluminescence (right) and absorbance (left) spectra of $Kb_{92.5}C7_{7.5}$ dissolved in 3 and 5mg/mL PMMA.

As seen in the table, these results have lower deviation, and thus the previous result for $Kb_{92.5}C7_{7.5}$ is discarded. Even though decreasing the PMMA content of the solution increases the PL maximum a little bit, a drop in the absorption maximum is also observed. Because maximum absorption values also affect the increment in the EQE of the device, a higher value is desired. Until this moment, the sample $Kb_{92.5}C7_{7.5}$ dissolved in 3mg/mL PMMA seems to be the sample with better properties as LDS filter. In order to verify that indeed this sample is close to the optimized sample, a last set of experiments near the optimized sample ($Kb_{92.5}C7_{7.5}$ in 3mg/mL PMMA) was done. For this set of measurements, a design of experiments using two factors and two different levels with three central points was carried out. The sample $Kb_{94}C7_6$ dissolved in 3mg/mL PMMA was chosen as the central point, and samples of $Kb_{92}C7_8$ and $Kb_{96}C7_4$ dissolved in 2 and 4 mg/mL were chosen as extreme points. Figure 25 shows the results of this design of experiments. Notice that the peaks of maximum absorbance and PL are smaller than the one obtained for the $Kb_{92.5}C7_{7.5}$ samples.
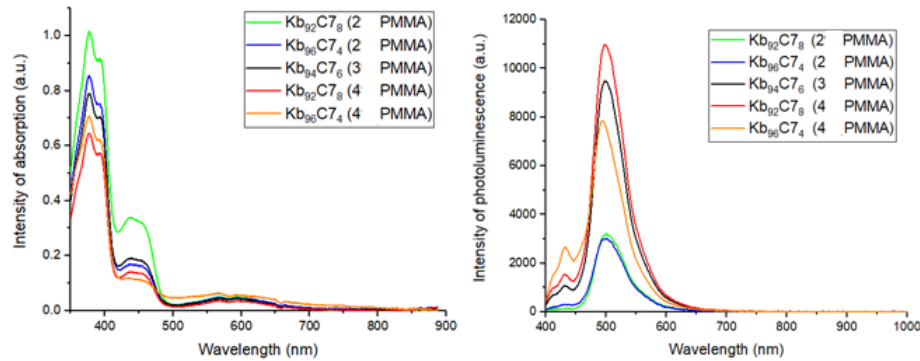

Figure 25 – Photoluminescence (right) and absorbance (left) spectra of different Kb-C7 samples dissolved in 2, 3 and 4mg/mL PMMA.

The following table summarizes the results of the design of experiments.

Table 5 – Design of experiments with three central points.

PMMA concentration (mg/mL)	sample	PLQY
2 (-)	$Kb_{92}C7_8(-)$	32
2 (-)	$Kb_{92}C7_8(-)$	31.4
2 (-)	$Kb_{96}C7_4(+)$	36.6
2 (-)	$Kb_{96}C7_4(+)$	27.3
4 (+)	$Kb_{92}C7_8(-)$	79.8
4 (+)	$Kb_{92}C7_8(-)$	84.5
4 (+)	$Kb_{96}C7_4(+)$	63.9
4 (+)	$Kb_{96}C7_4(+)$	60.9
3 (0)	$Kb_{94}C7_6(0)$	67.9
3 (0)	$Kb_{94}C7_6(0)$	64.8
3 (0)	$Kb_{94}C7_6(0)$	74.4
Mean		56.7

In order to calculate the effects of the factors, we use the same formulation used in the previous design of experiments. The data to be used is presented in the table:

Table 6 – Design of experiments for Kb-C7 samples with three central points.

PMMA concentration	Dyes concentration	1	2	3	PLQY value	variance
2 mg/mL (-)	$Kb_{92}C7_8(-)$	32	31.4	-	31.7 ±0.2	0.4
4 mg/mL (+)	$Kb_{92}C7_8(-)$	79.8	84.5	-	82.2 ±3.3	11.0
2 mg/mL (-)	$Kb_{96}C7_4(+)$	36.6	27.3	-	32.0 ±6.6	43.2
4 mg/mL (+)	$Kb_{96}C7_4(+)$	63.9	60.9	-	62.4 ±2.1	4.5
3 mg/mL (0)	$Kb_{94}C7_6(0)$	67.9	64.8	74.4	69.0 ±4.9	48.0

Based on the values of this table, we can calculate the effects of the factors and their interactions. Also, the central point offers a way to calculate residuals. The first thing we calculate is the variance, which is given by:

$$s^2 = \frac{df_1 v_1 + df_2 v_2 + df_3 v_3 + df_4 v_4 + df_5 v_5}{df_1 + df_2 + df_3 + df_4 + df_5}, \tag{4.11}$$

with df_i being the degrees of freedom of each level and v_i the variance of the respective level (i = 1,5). Replacing the values of the table, we get:

$$s^2 = \frac{0.4 + 11.0 + 43.2 + 4.5 + 2(48.0)}{6} = \frac{155.1}{6} = 25.85. \tag{4.12}$$

Notice the two additional degrees of freedom added by the central points to the statistics of this design of experiments. The error associated to the effects is given by:

$$s(effect) = \sqrt{\frac{s^2}{2}} = \sqrt{12.925} = 3.595. \tag{4.13}$$

The effect of PMMA concentration is given by:

$$C = \frac{-31.7 + 82.2 - 32.0 + 62.4}{2} = \frac{80.9}{2} = 40.45 \tag{4.14}$$

while the effect of dyes concentration is given by:

$$D = \frac{-31.7 - 82.2 + 32 + 62.4}{2} = \frac{-19.5}{2} = -9.75. \tag{4.15}$$

Finally, the effect of the interaction is given by:

$$CD = \frac{31.7 - 82.2 - 32 + 62.4}{2} = \frac{-20.1}{2} = -10.05. \tag{4.16}$$

The three central points add two degrees of freedom to our analyses, so the critical point for this design of experiments (with 95% confidence) is given by $t_6 = 2.447$. The significance is given by the error of the effects times the critical point $2.447 \times 3.595 = 8.797$. Because the absolute value of each effect is higher than this critical value, all the factors are significant for this design of experiments. Notice that for a given concentration of dyes, samples of 2 mg/mL PMMA concentration have lower PLQY values than samples dissolved in 4 mg/mL, showing that optimal PMMA concentration must be between 3 or 4 mg/mL. Also, for the samples with 4 mg/mL PMMA concentration, the sample with lower amount of Kb ($Kb_{92}C7_8$) has higher PLQY value than the sample with higher Kb content ($Kb_{96}C7_4$), but both PLQY values are smaller than the best value obtained for the sample $Kb_{92.5}C7_{7.5}$. These facts are in agreement with the previous results and give us confidence that indeed the sample $Kb_{92.5}C7_{7.5}$ dissolved in 3 mg/mL PMMA is closest to the real optimal sample, and this sample was chosen to be the optimal sample for applying in the $P3HT : PC61BM$ photovoltaic device.

4.2 Photoluminescence decay time measurements

In order to realize any energy transfer process, a set of photoluminescence decay time measurements was carried out. The excitation used was 375 nm, and two detection wavelengths, 440 and 510 nm, were used. The measurements were carried for three different Kb-C7 samples with the same PMMA concentration (1mg/mL). The samples selected were $Kb_{92}C7_8$, $Kb_{96}C7_4$ and $Kb_{98}C7_2$. The results are shown in figure 26, together with the decay curve of single Kb.
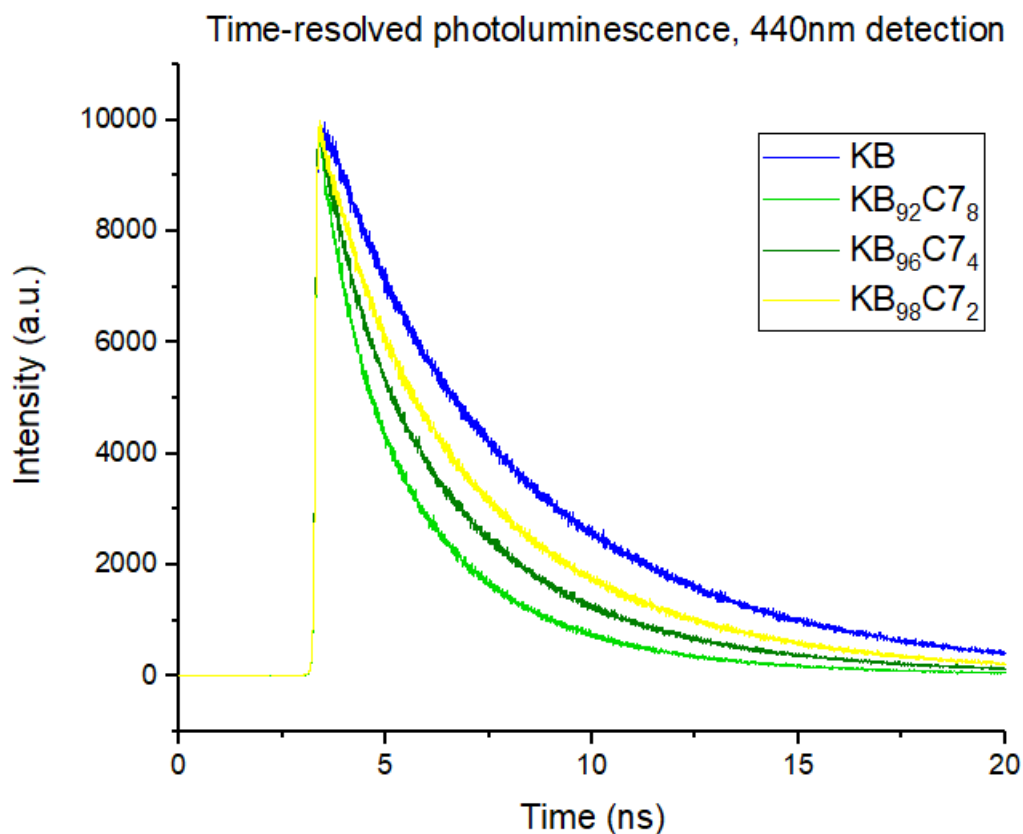
Time-resolved photoluminescence, 440nm detection

Figure 26 – Decay curve for Kb, $Kb_{92}C7_8$, $Kb_{96}C7_4$ and $Kb_{98}C7_2$ samples dissolved in 1 mg/mL PMMA. 375 nm excitation.

The average lifetime values for 440 and 510 nm excitation are shown in the following table, as well as the probability of energy transfer (see equation 2.26):

Table 7 – Decay lifetimes (amplitude weighted) of Kb-C7 samples dissolved in 1 mg/mL PMMA.

Samples	Avg. lifetime (440 nm)	Avg. lifetime (510 nm)	% of energy transfer (eq 2.26)
Kb	5.01 ns	–	–
$Kb_{98}C7_2$	4.15 ns	4.87 ns	17%
$Kb_{96}C7_4$	3.4 ns	4.17 ns	32%
$Kb_{92}C7_8$	2.55 ns	3.52 ns	49%

As we can see in the figure 26 and in table 7, there is a shift in the lifetime of the decay curve. The smaller is the Kb (donor) concentration, the shorter is the average lifetime of the mixed molecule, as expected from FRET theory. This is conclusive evidence that energy transfer between donor-acceptor molecules is occurring. The efficiency of energy transfer reported in the table was calculated under the assumption that donor molecules are isolated, and thus no homotransfer is taking place. This energy transfer is responsible for the observed increment in the PLQY values.

4.3 EQE simulations and I-V characteristic curve

Samples with better PLQY values were used to predict the EQE of devices using the LDS filter. As expected by Rothemund equation (2.23), the sample with highest PLQY value ($Kb_{92.5}C7_{7.5}$) was the sample that showed best performance when used as LDS filter in P3HT:PC61BM devices. Figure 27 shows a comparison between the reference and simulated EQE curves for this particular sample.
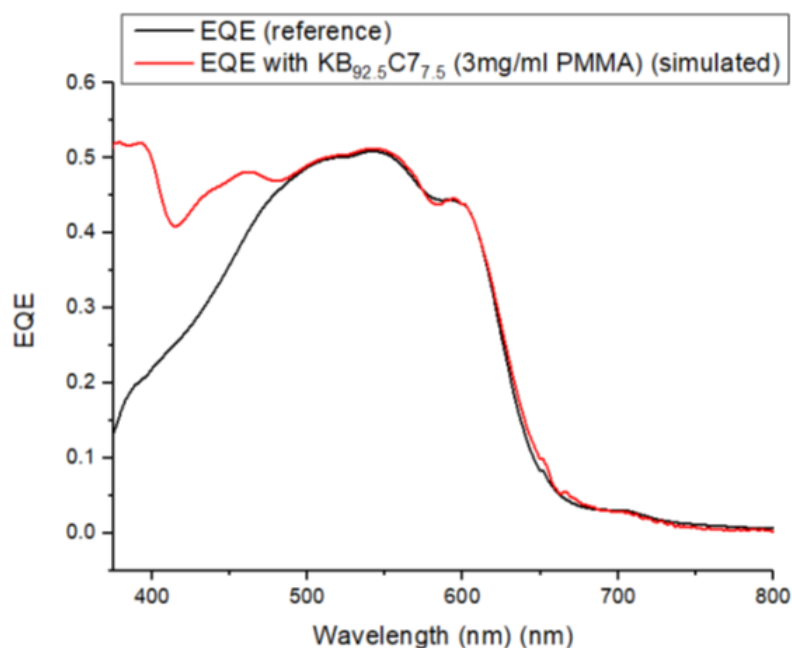

Figure 27 – Experimental EQE reference curve (black) of a P3HT:PC61BM device and simulated EQE curve (red) using the optimal LDS filter ($Kb_{92.5}C7_{7.5}$).

A clear increment in the EQE of the device near the UV region of the spectrum is observed. Simulations of the EQE in presence of the optimized LDS filter suggest an increase of 19.8% in the density of photogenerated current. In order to verify the validity of this prediction, a I-V characteristic curve test on 8 devices, with and without filter, was carried out. Figure 28 shows the results. The results show an average value of 18.6% in the increment of the photogenerated current, which is in agreement with the simulated results. A comparison of the I-V mean characteristic curve for the 8 devices, with and without the Kb-C7 optimal LDS filter, is shown in figure 29. It can be observed an slight increment in the open circuit voltage V_{OC} when using the LDS film in the photovoltaic device.
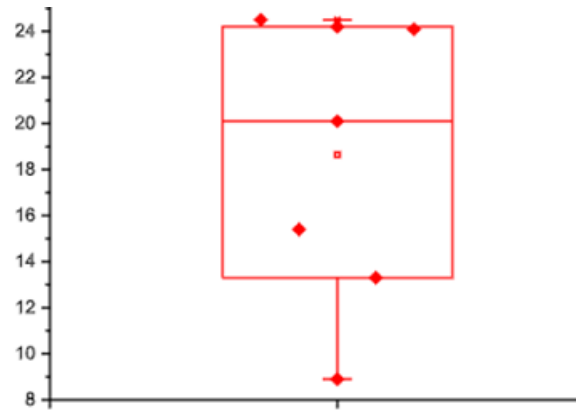
Figure 28 – Increment of photogenerated current (%) of 8 P3HT:PC61BM devices using the optimal LDS filter. The empty red square represents the average percentage of increment.
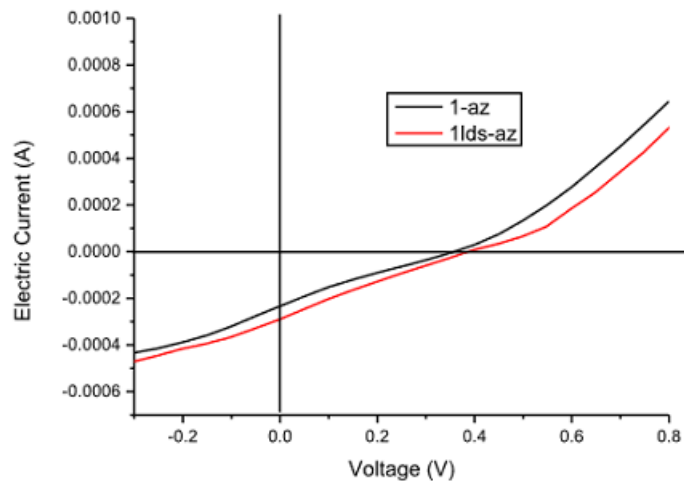
Figure 29 – I-V characteristic curve of P3HT:PC61BM devices, with and without LDS film (red and black curves, respectively).

4.4   Degradation test

Finally, a degradation test was carried out. It was measured the electric current density of two devices. The optimal LDS filter was applied to one of the devices, in order to see what is the effect of the LDS film in the degradation of the device. The samples were tested over a period of 24 hours of light exposure using a Xe lamp. The devices were not encapsulated. Figure 30 shows the comparison of the obtained results for both devices.
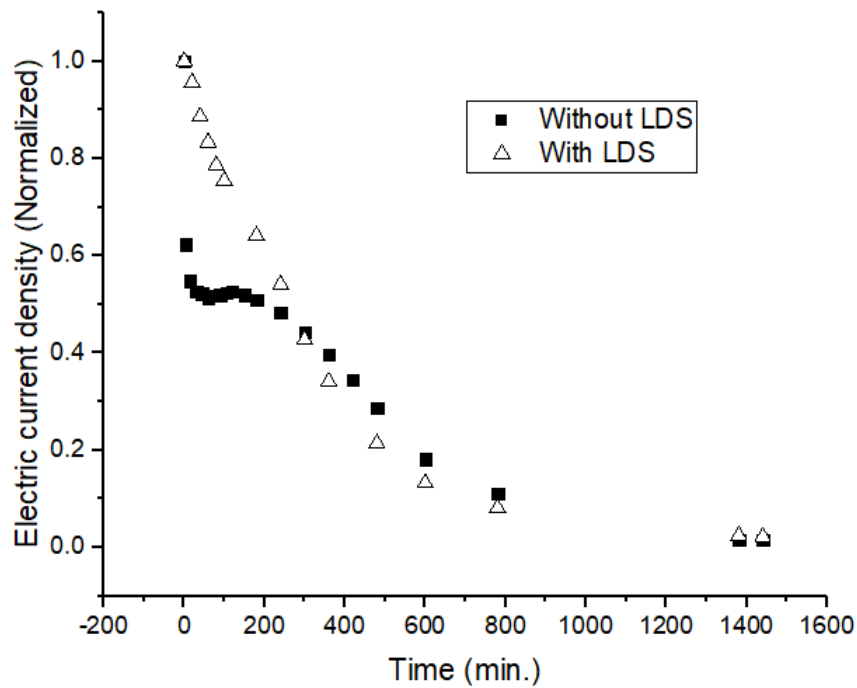
Figure 30 – Electric current density of P3HT:PC61BM devices, with and without optimal LDS filter (triangle and square curves, respectively).

During the first 200 minutes, the sample with the LDS filter displays higher current density values compared to the sample without filter. After that, the drop in the current density for both devices is similar. It is important to notice the rapid drop in the current density observed for the sample with no LDS filter. This could be caused by a previous oxidation of the active layer and/or the interface between the active layer and the Al electrode that is accelerated by UV radiation for the sample without the filter, while the same oxidation mechanism is delayed for the sample with the LDS filter, because it is blocking UV photons. However, no significant effect of the filter in the half-lifetime of the device is observed.

5 Conclusions

Production of various Kb-C7 samples with different dyes concentration dissolved in an optical inert matrix of PMMA with different concentrations, characterized by absorbance and PL measurements, show that it is possible to adjust the optical properties of the Kb-C7 LDS film by changing the mentioned parameters. It was found that the sample $Kb_{92.5}C7_{7.5}$ dissolved in 3mg/mL PMMA has a PLQY value of 93.6%, the highest value of Kb-C7 blends found in this work. This sample seems to be the optimal LDS film that contributes to enhancements in the EQE of P3HT:PC61BM devices, based on simulations carried out using the Rothemund model. The model predicts an increment of 19.8% in the photogenerated current. I-V characteristic curve measurements with 8 test devices show an average increment of 18.6% in the photogenerated current, which is in very good agreement with the theoretical prediction. Photoluminescence decay time measurements show a decrease in the lifetime of different Kb-C7 samples, supporting the fact that an energy transfer mechanism, presumably a Förster mechanism, is responsible for the increments in PLQY values. Finally, a degradation test of 24 hours of light exposure at ambient conditions was performed using P3HT:PC61BM devices, with and without the LDS film. The results show that during the first three hours of light exposure, photovoltaic devices made with the optimal Kb-C7 filter present higher current density values than clear devices. However, after three hours of exposure, the current density of both devices drops dramatically, indicating that some other factors like temperature, environment and moisture are inducing a rapid degradation in the device. Further test are needed, with encapsulated devices made under inert atmosphere conditions, to check the effect of the LDS layer as an UV filter.

Bibliography

[1] A. Ito, T. Oikawa, Global Mapping of Terrestrial Primary Productivity and Light-Use Efficiency with a Process-Based Model. Global Environmental Change in the Ocean and on Land. pp. 343–358.

[2] N. Apergisa, J. E. Payneb, Renewable and non-renewable energy consumption-growth nexus: Evidence from a panel error correction model.Energy Economics, Vol. 34, Issue 3, May 2012, pp. 733-738.

[3] J. W. Ngaira, Impact of climate change on agriculture in Africa by 2030. Scientific Research and Essays, Vol. 2 (7), July 2007, pp. 238-243.

[4] K. Kordesch, G. Simader, Fuel cells and their applications. ISBN 3-527-28579-2; TRN: DE96GC088, U.S. Department of Energy, Office of Scientific and Technical Information. Aug 01, 1996, 389 p.

[5] L. Yang, Z. Gang Chen, M. S. Dargusch, J. Zou, High Performance Thermoelectric Materials: Progress and Their Applications. Advanced energy materials, Vol. 8, Issue6, February 26, 2018, 1701797.

[6] Y. Wu, C. Cao, The way to improve the energy density of supercapacitors: Progress and perspective. Science China Materials, December 2018, Vol. 61, Issue 12, pp 1517–1526.

[7] H. Hosono, A. Yamamoto, H. Hiramatsu, Y. Ma, Recent advances in iron-based superconductors toward applications. Materials today, Vol. 21, Issue 3, April 2018, Pages 278-302.

[8] P. Cheng, G. Li, X. Zhan, Y. Yang, Next-generation organic photovoltaics based on non-fullerene acceptors. Nature photonics, https://doi.org/10.1038/s41566-018-0104-9.

[9] M. A. Green, Y. Hishikawa, E. D. Dunlop, D. H. Levi, J. H. Ebinger, A. W. Y. Ho-Baillie,Solar cell efficiency tables (version 52). Progress in photovoltaics, Vol. 26, Issue 7, July 2018 Pages 427-436.

[10] L. Meng, Y. Zhang, X. Wan1, C. Li, X. Zhang, Y. Wang, X. Ke, Z. Xiao, L. Ding, R. Xia, H. Lap Yip, Y. Cao, Y. Chen, Organic and solution-processed tandem solar cells with 17.3% efficiency. Science, Vol. 361, Issue 6407, 14 Sep 2018, pp. 1094-1098.

[11] J. A. Reinspach, Y. Diao, G. Giri, T. Sachse, K. England, Y. Zhou, C. Tassone, B. J. Worfolk, M. Presselt, M. F. Toney, S. Mannsfeld, Z. Bao, Tuning the Morphology of

Solution-Sheared P3HT:PCBM Films. ACS Applied Material Interfaces, January 15, 2016, pp. 1742-1751

[12] K. K. Chong, P. P. Khlyabich, K. J. Hong, M. R. Martinez, B. P.Rand, Y. LinLoob, Comprehensive method for analyzing the power conversion efficiency of organic solar cells under different spectral irradiances considering both photonic and electrical characteristics. Applied Energy, Vol. 180, 15 October 2016, pp. 516-523.

[13] Y. H. Lee, A. E. Abdu, D. H. Kim, T. W. Kim, Enhancement of the power conversion efficiency of organic photovoltaic cells due to AuSiO2 core shell nanoparticles embedded into a WO3 hole transport layer. Organic Electronics, Vol. 68, May 2019, pp. 182-186.

[14] B. G. A. L. Borges, A. G. Veiga, L. Tzounis, A. Laskarakis, S. Logothetidis, M. L. M. Rocco, Molecular Orientation and Ultrafast Charge Transfer Dynamics Studies on the P3HT:PCBM Blend. Journal of Physical Chemistry C, October 12, 2016, Vol 120, 43, 25078-25082.

[15] R. A. MarshJustin, M. Hodgkiss, S. Albert-Seifried, R. H. Friend, Effect of Annealing on P3HT:PCBM Charge Transfer and Nanoscale Morphology Probed by Ultrafast Spectroscopy. Nano Letters, February 2, 2010, pp. 923-930. https://doi.org/10.1021/nl9038289.

[16] W. Baek, H. Yang, T. Yoon, C. J. Kang, H. Lee, Y. Kim, Effect of P3HT:PCBM concentration in solvent on performances of organic solar cells. Solar Energy Materials and Solar Cells, Vol. 93, Issue 8, August 2009, pp. 1263-1267

[17] V. Shrotriya, Y. Yao, G. Li, Y. Yang, Effect of self-organization in polymer/fullerene bulk heterojunctions on solar cell performance. Applied Physical Letters, Vol 89, 063505 (2006), https://doi.org/10.1063/1.2335377.

[18] M. T. Dang, L. Hirsch, G. Wantz, P3HT:PCBM, Best Seller in Polymer Photovoltaic Research Advanced Materials, Vol. 23, Issue31, August 16, 2011, pp 3597-3602.

[19] B. T. de Villers, C. J. Tassone, S. H. Tolbert, B. J. Schwartz, Improving the Reproducibility of P3HT:PCBM Solar Cells by Controlling the PCBM/ Cathode Interface. Journal of Physical Chemistry C, 2009, 113, 18978–18982.

[20] Y. M. Yang, W. Chen, L. Dou, W. H. Chang, H. S. Duan, B. Bob, G. Li, Y. Yan, High-performance multiple-donor bulk heterojunction solar cells. Nature Photonics, 9 February 2015.

[21] T. Ameri, J. Min, N. Li, F. Machui, D. Baran, M. Forster, K. J. Schottler, D. Dolfen, U. Scherf, C. J. Brabec, Performance Enhancement of the P3HT/PCBM Solar

Cells through NIR Sensitization Using a Small-Bandgap Polymer. Advanced Energy Materials, Vol. 2, Issue10, October, 2012, pp. 1198-1202.

[22] K. Forberich, G. Dennler, M. C. Scharber, K. Hingerl, T. Fromherz, C. J.Brabec, Performance improvement of organic solar cells with moth eye anti-reflection coating. Thin Solid Films Vol. 516, Issue 20, 30 August 2008, pp. 7167-7170.

[23] A. Rivaton, S. Chambon, M. Manceau, J. L. Gardette, N. Lemaitre, S. Guillerez, Light-induced degradation of the active layer of polymer-based solar cells. Polymer Degradation and Stability, Vol. 95, Issue 3, March 2010, pp. 278-284.

[24] O. Moudam, N. Bristow, S. W. Chang, M. Horieb, J. Kettle, Application of UV-absorbing silver(I) luminescent down shifter for PTB7 organic solar cells for enhanced efficiency and stability.

[25] R. V. Fernandes, A. Urbano, J. L. Duarte, N. Bristow, J. Kettle, E. Laureto, Tuning the optical properties of luminescent down shifting layers based on organic dyes to increase the efficiency and lifetime of P3HT:PCBM photovoltaic devices. Journal of Luminescence, Vol. 203, November 2018, pp. 165-171.

[26] R. V. Fernandes, N. A. Cordeiro, A. D. P. Perdomo, J. L. Duarte, E. Laureto, Optimizing the optical properties of a dye-based luminescent down-shifter to improve the performance of organic photovoltaic devices. Dyes and Pigments, Vol. 169, October 2019, pp. 1-6.

[27] R. V. Fernandes, N. Bristow, V. Stoichkov, H. S. Anizelli, J. L. Duarte, E. Laureto, J. Kettle, Development of multidye UV filters for OPVs using luminescent materials. Journal of Physics D: Applied Physics, Vol 50, (2017) 025103 (8pp).

[28] R. V. Fernandes, Aplicação de materiais com luminescência deslocada para menores energias em dispositivos fotovoltaicos orgânicos de P3HT:PCBM. Tese de Doutorado, Departamento de Física da Universidade Estadual de Londrina, 2018.

[29] C. Kittel, Introduction to solid state physics. John Wiley and Sons; Edição: 8th (11 de novembro de 2004). ISBN-13: 978-0471415268

[30] H. D. Young, R. A. Freedman, Física IV - Óptica e Física Moderna. Pearson Addison Wesley, 2008. 12a. edição, ISBN 978-85-88639-35-5

[31] W. Struve, Fundamentals of molecular spectroscopy. Wiley-interscience publication ISBN 539.6 88-5459, 1989. 379 pages.

[32] P. A. Tipler and R. A. Llewellyn, modern physics, 5th edition. W. H. Freeman and Company 41 Madison Avenue New York, NY 10010 Houndmills, Basingstoke RG21 6XS, England www.whfreeman.com, ISBN-10: 0-7167-7550-6

[33] R. F. Pierret, semiconductor device fundamentals. Adison Wesley publishing company, 1996, ISBN 0-201 54395-1.

[34] S. M. Rezende, Materiais e Dispositivos Eletrônicos, Editora Livraria da Física, 2004. ISBN 85-88325-27-6

[35] J. Nelson, the physics of solar cells. Imperial College press, London WC2H 9HE, 2003. ISBN-13 978-1-86094-340-9.

[36] N. Marinova, S. Valero, J. L. Delgado, Organic and perovskite solar cells: working principles, materials and interfaces. Journal of Colloid and Interface Science, vol. 488, p. 373-389, 2017.

[37] https:en.wikipedia.org/wiki/Theoryofsolarcells, taken September 25, 2019.

[38] E. Hecht, Optics, 4th edition. Adelphi University, 2002.ISBN-13: 9780805385663.

[39] B. Valeur, Molecular Fluorescence: Principles and Applications. 2001 Wiley-VCH ISBNs: 3-527-29919-X (Hardcover); 3-527-60024-8 (Electronic).

[40] A. Solodovnyk, C. Kick, A. Osvet, H. J. Egelhaaf, E. Stern, M. Batentschuk, K. Forberich, C. J. Brabec, Optimization of Solution-Processed Luminescent Down-Shifting Layers for Photovoltaics by Customizing Organic DyeBased Thick Films. Energy Technology, doi:10.1002/ente.201500404.

[41] R. .Rothemund, Optical modelling of the external quantum efficiency of solar cells with luminescent down-shifting layers. Solar Energy Materials and Solar Cells, Vol. 120, Part B, January 2014, pp. 616-621.

[42] B. de Barros Neto, I. S. Scarminio, R. E. Bruns, como fazer experimentos, pesquisa e desenvolvimento na ciência e na indústria. Copyright by Editora da Unicamp. 2001.

[43] http://www.shimadzu.com.br/analitica/produtos/spectro/uv/uv-3600-plus.shtml

[44] J. C. de Mello, H. F. Wittmann, R. t. Friend, An Improved Experimental Determination of External Photoluminescence Quantum Efficiency. Advanced Materials Communications. 1997 0935-9648/97/0302-O230.

[45] https:www.picoquant.com/applications/category/materials-science/time-resolved-photoluminescence